Cell Reports
Physical Science

Article

Engineering the glioblastoma microenvironment using TLR7/8 agonist-complexed graphene oxide nanosheets

Graphical abstract

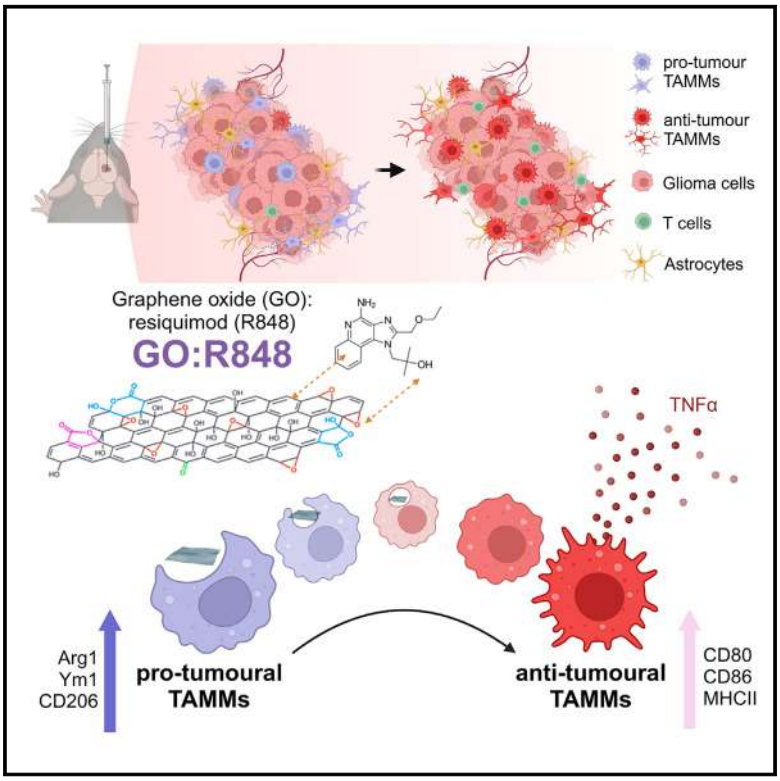

Highlights

- Thin graphene oxide (GO) nanosheets are complexed with an immunostimulatory agonist
- GO complexes are selectively internalized by tumor-associated macrophages
- This acts to reprogram the wider glioblastoma immune microenvironment
- GO-complex-mediated immunomodulation suppresses tumor growth

Authors

Maria Stylianou, Thomas Kisby, Despoina Despotopoulou, ..., Neus Lozano, Andrew S. MacDonald, Kostas Kostarelos

Correspondence

thomas.kisby@manchester.ac.uk (T.K.), kostas.kostarelos@manchester.ac.uk (K.K.)

In brief

The tumor microenvironment of aggressive brain tumors is immunosuppressive, which can support their growth and progression. Stylianou et al. show that through delivery of graphene oxide nanosheets complexed with an immunostimulatory agonist, they can reprogram the immune microenvironment of glioblastoma and suppress tumor growth.

Stylianou et al., 2025, Cell Reports Physical Science 6, 102342
January 15, 2025
https://doi.org/10.1016/j.xcrp.2024.102342

CellPress

Cell Reports
Physical Science

CellPress
OPEN ACCESS

Article

Engineering the glioblastoma microenvironment using TLR7/8 agonist-complexed graphene oxide nanosheets

Maria Stylianou,[1,2] Thomas Kisby,[1,2,*] Despoina Despotopoulou,[3] Helen Parker,[4] Alexandra Thawley,[1] Kiana Arashvand,[1] Neus Lozano,[3] Andrew S. MacDonald,[4] and Kostas Kostarelos[1,2,3,5,6,*]

[1]Nanomedicine Lab, Centre for Nanotechnology in Medicine, Faculty of Biology, Medicine & Health, University of Manchester, AV Hill Building, Manchester M13 9PT, UK

[2]Geoffrey Jefferson Brain Research Centre, Manchester Academic Health Science Centre, Northern Care Alliance NHS Foundation Trust, University of Manchester, Manchester, UK

[3]Nanomedicine Lab, Catalan Institute of Nanoscience and Nanotechnology (ICN2), CSIC and BIST, Campus UAB Bellaterra, 08193 Barcelona, Spain

[4]Lydia Becker Institute of Immunology and Inflammation, Faculty of Biology, Medicine and Health, University of Manchester, Manchester, UK

[5]Institució Catalana de Recerca i Estudis Avançats (ICREA), Pg. Lluís Companys 23, Barcelona, Spain

[6]Lead contact

*Correspondence: thomas.kisby@manchester.ac.uk (T.K.), kostas.kostarelos@manchester.ac.uk (K.K.)

https://doi.org/10.1016/j.xcrp.2024.102342

SUMMARY

The glioblastoma (GBM) microenvironment is immunologically "cold" and marked by immunosuppressive components that limit the effectiveness of current immunotherapies. Tumor-associated macrophages and microglia (TAMMs) exist in an immunosuppressive state and contribute to this "coldness," promoting tumor progression and resistance to therapy. Traditional macrophage reprogramming strategies face challenges in delivery and retention of agents within the GBM microenvironment, leading to limited clinical success. This study investigated whether two-dimensional graphene oxide (GO) nanosheets can enhance the delivery of a TLR7/8 agonist (R848) to TAMMs. GO effectively delivered R848, enhancing TAMM reprogramming from an M2-like to an M1-like state *in vitro*. In a syngeneic mouse model, GO:R848 treatment significantly increased M1-like markers (MHCII, CD86, and TNF-α), reduced M2-like markers (ARG1 and YM1), increased T cell infiltration, and inhibited tumor progression. These findings demonstrate that GO nanosheets can improve the selective local delivery of immunomodulatory agents and alter the immune landscape of GBM.

INTRODUCTION

The tumor microenvironment (TME) plays a key role in glioblastoma (GBM) invasiveness, resistance, and rapid progression. Despite tremendous efforts to develop novel therapies including immunotherapies, GBM has evolved multiple mechanisms to escape immune surveillance that compromise the efficacy of these investigative drugs, with median survival remaining at only 15–16 months after diagnosis.[1–3]

In GBM, monocyte-derived macrophages recruited from bone-marrow and brain-resident macrophages known as microglia (tumor-associated macrophages and microglia [TAMMs]) are highly abundant immune cells that comprise 30%–40% of the tumor.[4,5] Macrophage polarization is heterogeneous, with differential activation states between a pro-inflammatory/classic (M1-like) and an anti-inflammatory/alternative (M2-like) state. M1-like macrophages are responsible for pathogen and cell debris removal and have anti-tumorigenic properties, whereas M2-like macrophages promote tissue repair and have been shown to facilitate tumor proliferation.[4,6–10] In the context of gliomas, abundance of M1-like anti-tumoral TAMMs have been correlated with low-grade gliomas, while increased M2-like pro-tumoral TAMMs have been found in high-grade gliomas and correlate with aggressiveness and poor survival.[11,12] Therefore, modulating this population of TAMMs to increase M1-like anti-tumoral macrophages and reduce M2-like pro-tumoral populations has attracted great interest as an adjunctive therapy in high-grade gliomas such as GBM.

Based on this understanding, strategies such as TAMM reprogramming have been explored alone or in combination with other immunotherapies and have demonstrated improved therapeutic effects in some GBM pre-clinical models.[13,14] One of those strategies is the stimulation of Toll-like receptors (TLRs) using TLR agonists, which leads to favorable changes in macrophage phenotype and increases their phagocytic and cancer cell clearance activity. Additionally, such stimulation could facilitate activation of adaptive immunity and support cytotoxic $CD8^+$ T cell responses.[15,16] TLR7 agonists include native single-stranded RNA viruses and synthetic small molecules such as imidazoquinolines.[17] Through TLR-mediated signaling

cascades, these molecules activate nuclear factor κB, leading to transcription of pro-inflammatory genes in various innate immune cells, including macrophages, microglia, and dendritic cells. The imidazoquinoline family includes the US Food and Drug Administration-approved topical imiquimod (Aldara) and its more effective counterpart resiquimod (R848), which possesses 10-fold greater pro-inflammatory activity.[18] Although there are limited studies that have introduced R848 intracranially or systemically in GBM,[19–22] it has been shown to have a potent immunomodulatory activity and exert an anti-tumor effect in skin malignancies, including melanoma and squamous cell carcinomas.[18,23] Furthermore, R848 has been demonstrated to reprogram TAMMs from an M2-like pro-tumoral to an M1-like anti-tumoral phenotype in multiple solid tumors.[24–26] However, due to limited capacity of these molecules to bypass the blood-brain barrier (BBB), poor entry and retention in the tumor site, and compensatory high dosing leading to systemic immunotoxicities, the clinical translation of TAMM modulation strategies has been limited, particularly in intracranial tumors.[27–30] Due to these challenges, local (intratumoral) delivery strategies have been largely employed for brain tumors, which, while bypassing delivery issues associated with the BBB and enabling lower doses, have not yet demonstrated clear efficacy in patients.[27,31]

The use of nanoparticles to deliver drugs directly to the tumor site can not only prolong release of the drug locally but can also improve TAMM targeting and reduce off-target systemic side effects that have been limiting to clinical translation.[32–35] In other types of solid tumors, R848 encapsulated within nanoparticles has been demonstrated to be a potent driver of the M1-like anti-tumoral phenotype and tumor-associated macrophage activation.[36–38] For instance, in breast cancer it has been demonstrated that β-cyclodextrin nanoparticles encapsulating R848 lead to significantly increased pro-inflammatory cytokines in tumor-associated macrophages, with a change toward an M1-like phenotype.[25] Graphene oxide (GO) nanosheets could be a potent platform for transport and presentation of immunomodulatory drugs in GBM, considering the large available surface area and proven *in vivo* biocompatibility[39–42] without any neural toxicity.[43,44] Previously, we have demonstrated that GO nanosheets diffuse spontaneously throughout the tumor area of GBM without traversing its borders into the brain after a single intratumoral injection.[45] In addition, we have illustrated that GO is taken up primarily by IBA1$^+$ macrophages and microglia within the TME.[45,46] Others have previously used cationic polymer (PEI)-modified GO to form complexes with R848 and nucleic acids[47,48] to demonstrate vaccine-adjuvant activity in dendritic cells and macrophages *in vitro*. We have instead engineered a simpler, thinner complex between bare, medical-grade, endotoxin-free GO and R848 as a possible immunomodulatory platform appropriate for *in vivo* applications.[49]

In this work, we investigated thin GO nanosheets as a platform to selectively deliver the TLR7/8 agonist, R848, into TAMMs *in vivo* as a strategy to alter the immunosuppressive character of the GBM TME. We prepared and characterized GO:R848 complexes and evaluated their capability to reprogram M2-like macrophages toward M1-like macrophages. We then utilized an orthotopic, syngeneic GL261 mouse model to investigate the distribution and the *in vivo* reprogramming of TAMMs via GO:R848. We found that a single low-dose intratumoral administration of GO:R848 could significantly elevate M1-like anti-tumoral markers and alter the wider GBM landscape with more prolonged activity compared to R848 alone. Additionally, we showed that this approach could suppress tumor growth *in vivo*, providing evidence that GO:R848 can therapeutically modulate the highly immunosuppressive character of aggressive brain tumors.

RESULTS

Characterization of a non-covalent GO:R848 nanocomplex

Complexes between GO nanosheets and the R848 small molecule (GO:R848) were prepared by orderly mixing of the two components in an aqueous suspension as described (Table S1).[49] Following incubation, we characterized size (lateral dimensions) via atomic force microscopy (AFM) and scanning electron microscopy (SEM), which demonstrated the retention of single GO flakes without significant alteration of lateral dimensions (Figures 1 and S1). We further studied the colloidal stability and pH variation over time in water (long-term storage vehicle) and in 5% dextrose (*in vivo* injection vehicle) for 8 days and 24 h, respectively. GO:R848 and the equivalent GO-alone control remained stable over time without any significant alteration in mean particle dimensions, surface charge, or pH (7.5 pH), including with the addition of 5% dextrose just prior to injection (Figure S2), confirming a stable complex system suitable for further biological investigation.

GO:R848 retains capacity for differentiation of M0 to M1-like macrophages *in vitro*

To evaluate whether complexation of R848 with GO retains its biological activity, we assessed the capacity of GO:R848 to promote differentiation of M0 macrophages to M1-like macrophages. We validated the capacity of R848 to induce tumor necrosis factor α (TNF-α) production (as a marker of M1-like activation) by naive mouse bone-marrow-derived macrophages (BMDMs) (Figure S3). We next confirmed the uptake of both GO and GO:R848 (equivalent to 0.01 μg R848), which demonstrated a high degree of internalization in macrophages by Raman spectroscopy (Figures 2A and S4). We also confirmed that GO or GO:R848 did not cause any toxicity to primary macrophages (Figure S5A) or acute toxicity to cancer cells, microglia, or neuronal cell lines, indicating good biocompatibility (Figure S5B). To assess the biological response to GO:R848, we utilized phalloidin staining to observe macrophage morphology, as it has been highlighted as a complementary biomarker for cellular function/activation state.[25,50] We observed that GO:R848 appeared to induce the phenotypic differentiation of M0 to M1-like macrophages (Figures 2B and S6). We further examined this molecularly, using CD206 and CD80 membrane markers as M2-like and M1-like activation markers, respectively.[51] GO:R848 significantly elevated the proportion of CD80$^+$ macrophages, and CD80 expression within this population (gMFI) compared to both untreated (M0) and M2-like (interleukin-10 [IL-10]/IL-4 stimulated) negative control and sustained

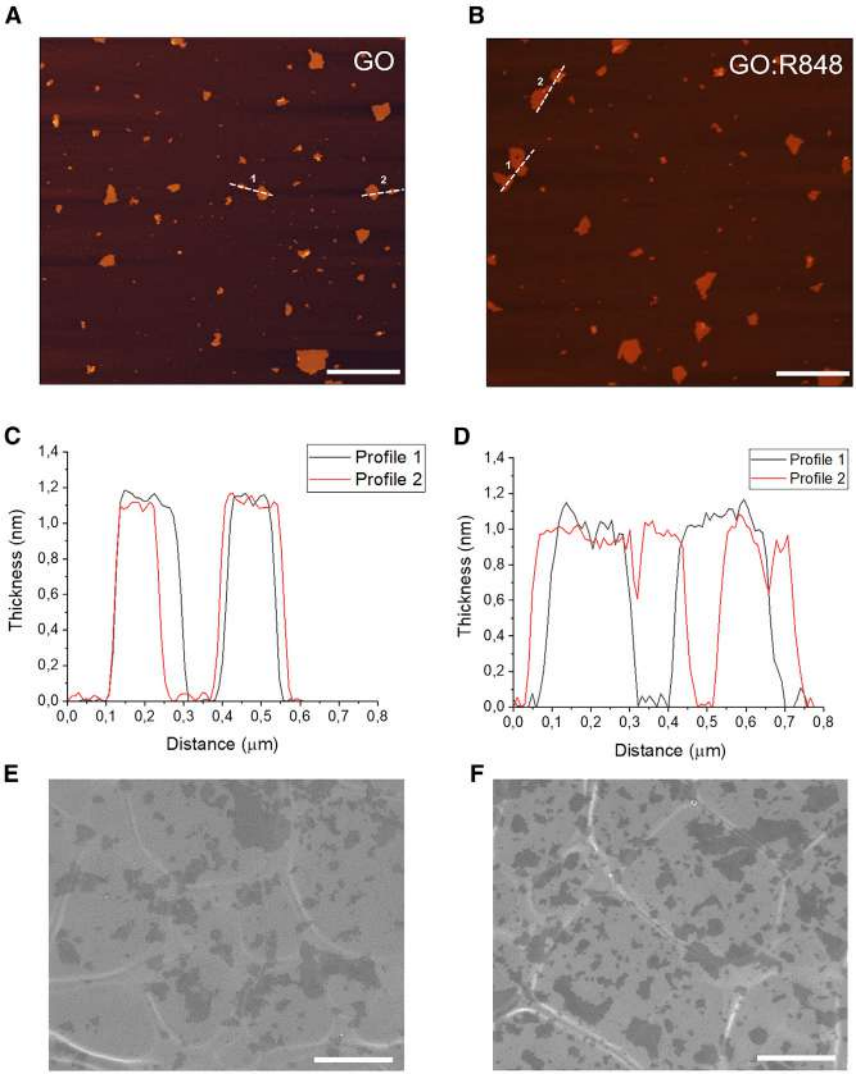

Figure 1. Morphological characterization of GO and GO:R848 complex

(A and B) AFM images with corresponding flake cross-section for GO control (A) and GO:R848 (B). (C and D) Thickness profiles based on AFM images of GO (C) and GO:R848 (D). $n = 2$ flakes/profile. (E and F) SEM images of GO (E) and GO:R848 (F). Scale bars, 1 μm.

the proportion of CD206$^+$ macrophages and CD206 expression at low levels, consistent with untreated M0 macrophages, confirming an M0 to M1-like differentiation (Figure 2C). This confirmed that R848 remains active following complexation onto GO. Further to this, macrophages treated with GO:R848 showed significantly elevated levels of TNF-α production compared to both free R848 and the negative controls (Figure 2D), indicating that the GO nanocomplex may enhance differentiation of M1-like macrophages even more so than the TLR agonist alone.

GO:R848-mediated reprogramming of M2- to M1-like macrophages *in vitro*

To examine the *in vitro* reprogramming of macrophages, we pretreated BMDMs for 24 h with an IL-10/IL-4 cytokine cocktail to drive them toward an M2-like phenotype, as confirmed by immunostaining for CD206 (Figure 3A), before further treatment with GO:R848 or controls. Initially, using phalloidin staining and bright-field microscopy, we illustrated morphological alteration to a circular, M1-like phenotype when M2-like macrophages were treated with GO:R848 that matched the morphology of macrophages treated with lipopolysaccharide (LPS)/interferon-γ (IFN-γ) (Figures 3B and S7). We further confirmed that GO:R848 significantly attenuated the proportion of CD206$^+$ macrophages (M2-like) and raised the expression of CD80 (gMFI) compared to the M2-like control group, something that we did not observe with the free R848 control (Figure 3C). To further validate these results, we measured TNF-α cytokine levels 24 h post treatment (48 h post pre-differentiation to M2-like) and demonstrated that GO:R848 showed significantly increased M1-like cytokine production compared to free R848 and controls, again without any apparent toxicity (Figures 3D and S8). Interestingly, despite their M2-pre-differentiation, these cells showed an increased cytokine production response to pro-inflammatory stimuli including GO:R848, highlighting the plasticity of macrophage polarization. These results confirmed that GO:R848 can effectively reprogram M2-like macrophages to a more inflammatory M1-like state and further indicates that GO nanosheet complexes retain and may provide enhancement of the activity of R848.

GO:R848-treated macrophages retain phagocytic ability

To interrogate whether macrophages loaded with the GO:R848 complex can conserve their phagocytic ability, we performed a phagocytic assay utilizing fluorescent beads. Following treatment of BMDMs with GO:R848 and controls for 24 h, we cultured cells with fluorescent beads for 1 h and evaluated phagocytosis via flow cytometry based on the proportion of macrophages positive for beads (Figure S9A). Importantly, GO:R848-treated macrophages retained their phagocytic ability in terms of proportion of bead$^+$ macrophages and had enhanced phagocytic capacity compared to IL-4/IL-10-treated M2-like macrophages (Figure S9B). These data suggested that macrophage uptake of GO:R848 does not disrupt their phagocytic function and further induces M1-like differentiation with the elevated phagocytic activity associated with this polarized state.

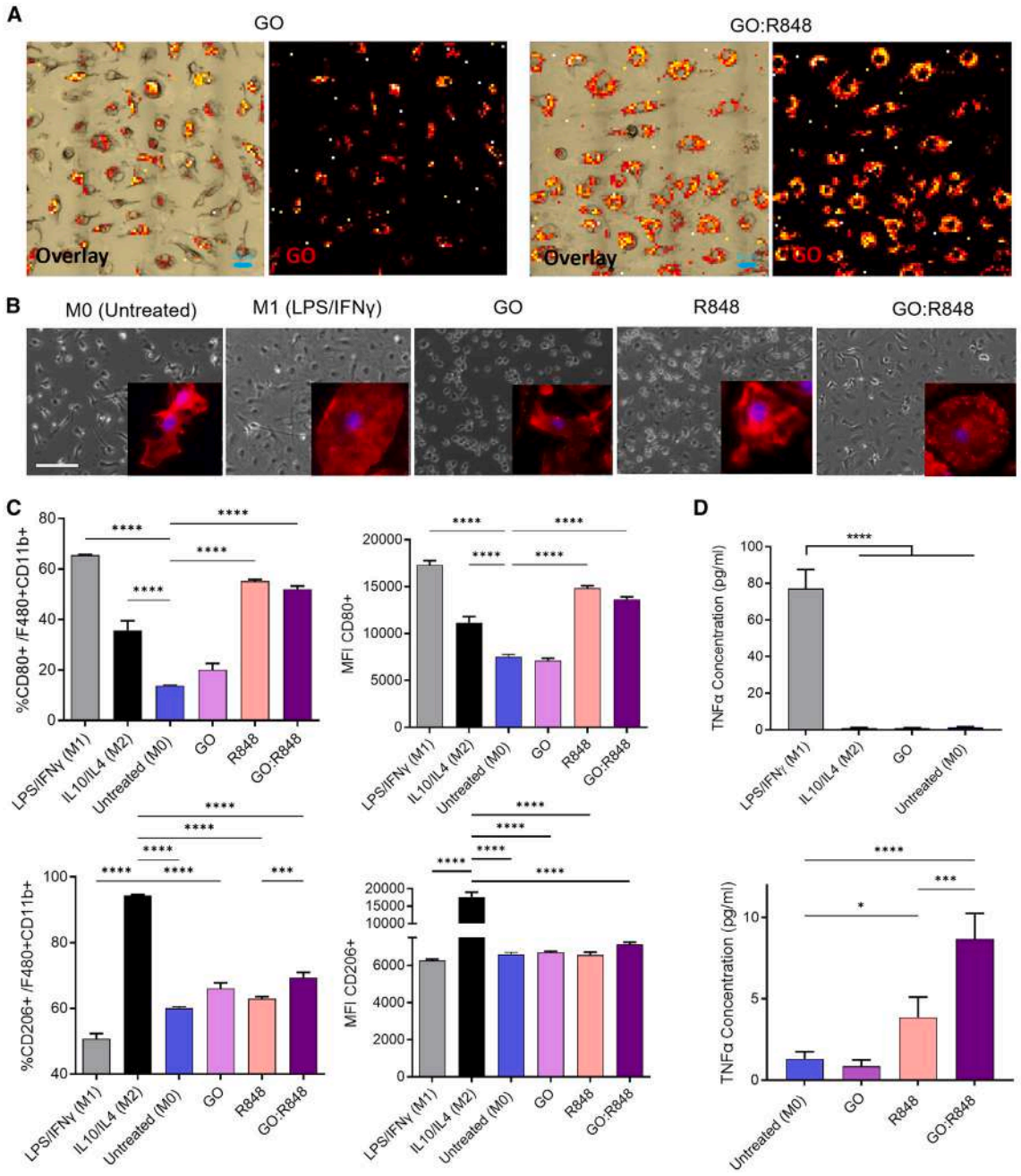

Figure 2. GO:R848 mediated differentiation of M0-like macrophages to M1-like macrophages

(A) Raman spectroscopy and optical overlay images of GO Raman signal 24 h post exposure to GO (10 μg) or GO:R848 (10 μg). Scale bars, 20 μm.

(B) Phase-contrast images of macrophages 24 h post treatment with LPS (100 ng)/IFN-γ (20 ng), M1-like anti-tumoral phenotype, GO (10 μg), R848 (0.01 μg), or GO:R848 (10 μg: 0.01 μg). Scale bar, 100 μm. Zoomed-in single-cell immunofluorescence images showing single-cell phenotype. Phalloidin-actin cytoskeleton, red; DAPI nuclei, blue.

(C) Percentage of $CD80^+$ and $CD206^+$ (left panels) out of $F480^+/CD11b^+$ cells and corresponding geometric MFI (gMFI) of these markers (right panels), 24 h post treatment, measured by flow cytometry.

(D) TNF-α concentration (pg/mL) from supernatant of macrophages 24 h post treatment with GO, R848 (0.01 μg), or GO:R848 (10 μg: 0.01 μg), or controls.

Data are presented as mean ± SD, $n = 3$ biological replicates. One-way ANOVA with Tukey's multiple-comparison test (*$p < 0.05$, ***$p < 0.001$, ****$p < 0.0001$).

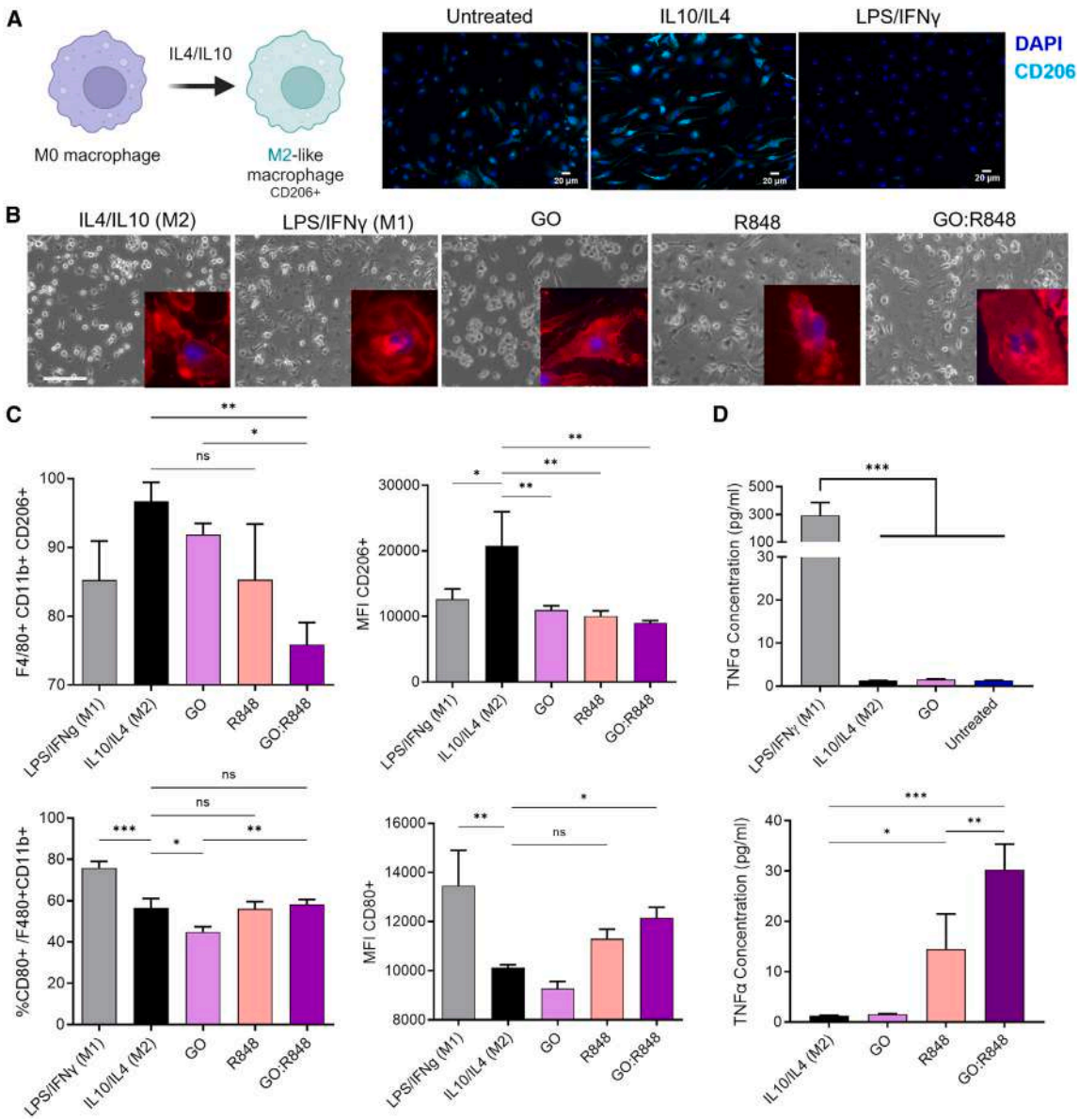

Figure 3. GO:R848 induced reprogramming of M2-like to M1-like macrophages

(A) BMDMs were first pre-treated for 24 h with IL-10/IL-4 to differentiate them to an M2-like phenotype, which was confirmed by increased expression of CD206. Scale bar, 20 μm.

(B) Phase-contrast images taken 24 h post treatment with LPS (100 ng)/IFN-γ (20 ng), GO (10 μg), R848 (0.01 μg), or GO:R848 (10 μg:0.01 μg) Scale bar, 100 μm. Zoomed-in single-cell immunofluorescence images showing cell phenotype. Phalloidin-actin cytoskeleton, red; DAPI nuclei, blue.

(C) Flow-cytometry charts showing the percentage of $CD206^+$ and $CD80^+$ out of $F480^+/CD11b^+$ population and the corresponding geometric MFI 24 h post treatment.

(D) TNF-α concentration (pg/mL) in supernatant of M2-like differentiated BMDMs 24 h post treatment (48 h after pre-treatment) with GO, R848 (0.01 μg), GO:R848 (10 μg:0.01 μg), or controls.

Data are presented as mean ± SD, $n = 3$ biological replicates. One-way ANOVA with Tukey's multiple-comparison test (*$p < 0.05$, **$p < 0.01$, ***$p < 0.001$; ns, not significant).

In vivo distribution of GO:R848 and selective TAMM uptake

Having demonstrated *in vitro* macrophage reprogramming, we sought to investigate the *in vivo* distribution of GO:R848 after a single local administration into GBM tumors in a syngeneic GL261 mouse model. Tumors were generated by intracranial inoculation with 5×10^4 GL261-luc cells (day 0), followed with intratumoral injection of GO:R848 (10:4 mass ratio, 0.72 μg R848) on day 5 (Figure 4A). Histological analysis of brains on days 1, 2, 5, and 10 post treatment (days 6, 7, 10, and 15 of tumor growth)

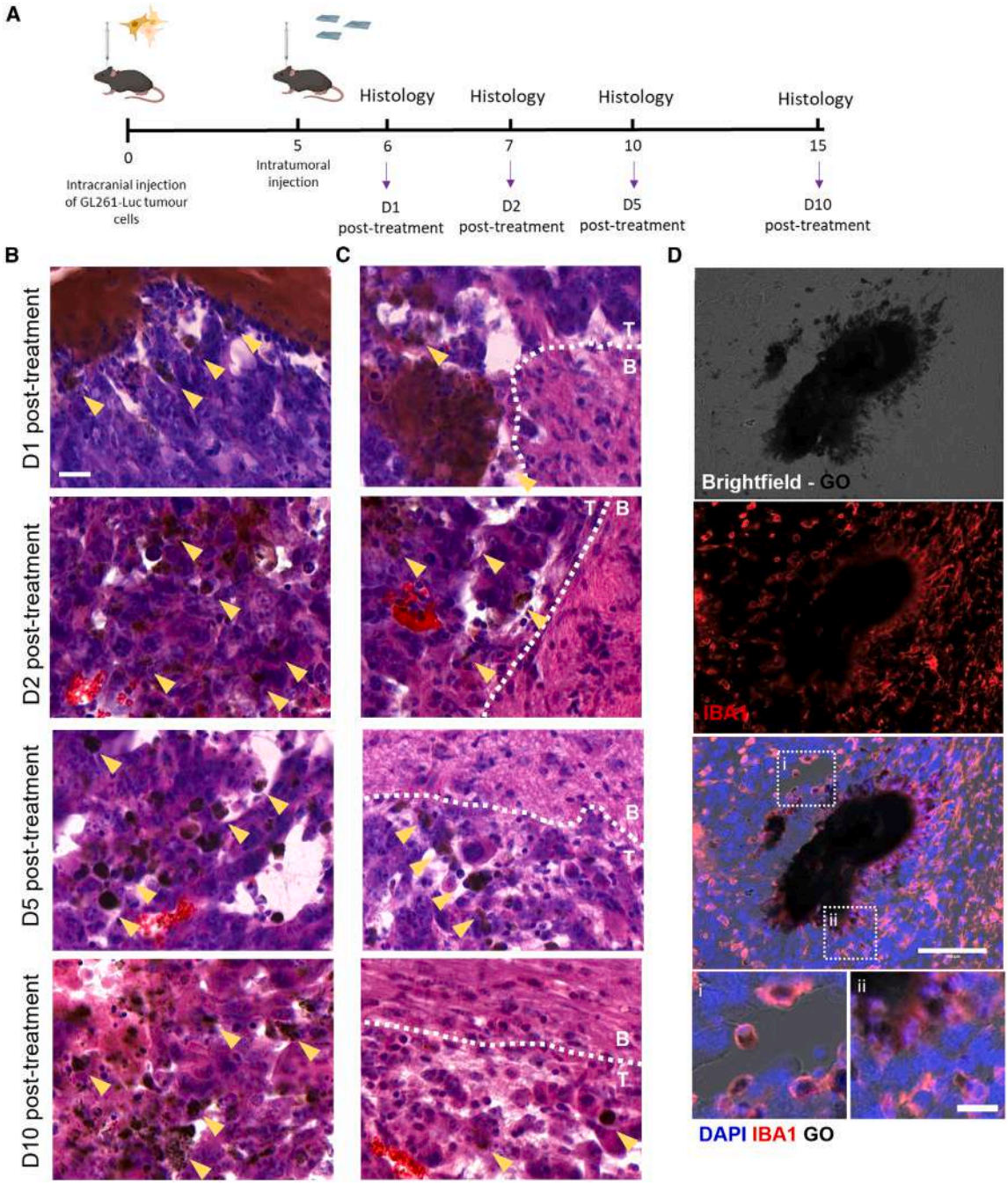

Figure 4. *In vivo* GO:R848 complex distribution in GBM tumors over time

(A) Experimental schematic illustrating the design of the *in vivo* experiment. C57Bl/6 mice were implanted with 5×10^4 (1 μL) GL261-luc cells into the right striatum (intracranial; i.c.). Five days following tumor inoculation, mice were treated by intratumoral (i.t.) delivery of 5% dextrose, R848 (0.72 μg), or GO:R848 (10:4; 1.8 μg:0.72 μg).

(B) Representative H&E-stained sections at 1, 2, 5, and 10 days post GO:R848 treatment showing presence of GO^+ (dark brown) cells (yellow arrowheads). Scale bar, 20 μm.

(C) Representative H&E-stained sections at the tumor edge (dashed line) showing presence of GO^+ (dark brown) cells (yellow arrowheads) within the tumor (T) but not the brain (B). Scale bar, 20 μm.

(D) Overlaid bright-field and immunofluorescence images showing co-localization of GO^+ signal (black) with $IBA1^+$ cells (macrophages/microglia) 5 days post administration of GO:R848. Scale bars, 100 μm (D) and 20 μm (Di, Dii).

Images representative of $n = 4$ mice/group.

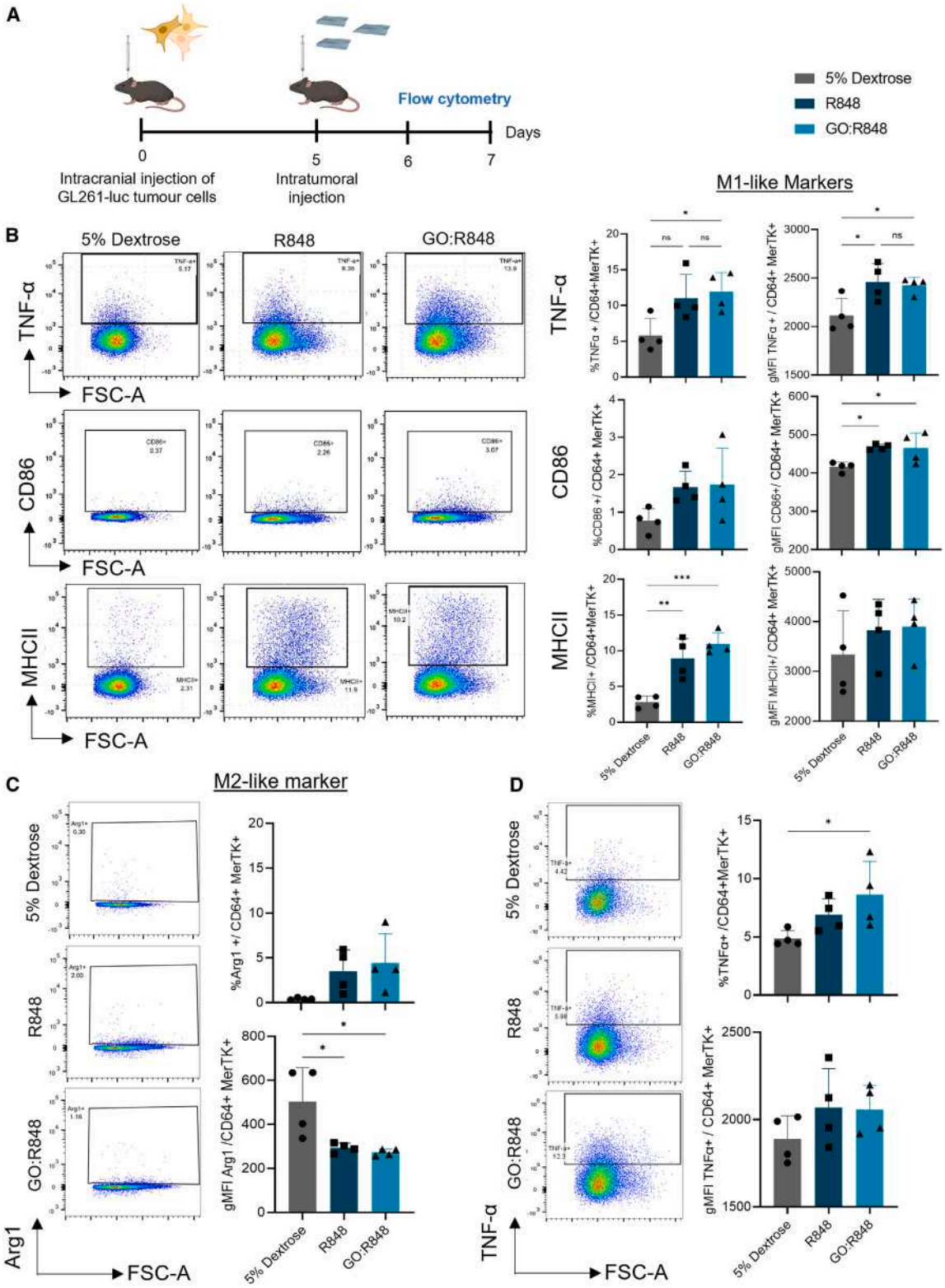

(legend on next page)

were performed, and the distribution of the GO:R848 complex was monitored based on the dark-brown appearance of GO visible by light microscopy. Based on microscopy of H&E-stained sections, we observed the gradual redistribution of GO:R848 away from the initial site of injection between days 1 and 5, coinciding with the presence of cells throughout the TME that appeared highly loaded with GO (Figures 4B and S10). Notably, no GO:R848 was detected outside the tumor border, consistent with our previous findings[45] and highlighting the inherent tumor-selective nature of GO nanosheets (Figure 4C). Through further immunofluorescence analysis, we confirmed that IBA1$^+$ TAMMs, which rapidly infiltrate the site of injection (Figures S10C and S11), were the primary carriers (>75%) of GO and GO:R848 (Figures 4D and S12). These results demonstrate that locally administered GO complexes can passively target TAMMs present in the GBM TME and therefore may offer advantages as a tumor-localized TAMM-selective delivery system.

In vivo modulation of TAMMs and alteration of GL261 microenvironment landscape

As IBA1$^+$ TAMMs were the major cell component interacting with GO:R848, we hypothesized that we could utilize this complex to reprogram these cells from an M2-like pro-tumoral to an M1-like anti-tumoral state within the TME. To evaluate the *in vivo* modulation of TAMMs in the GBM microenvironment, we generated tumors as described above and administered a single intratumoral injection of GO:R848 (1.8 μg:0.72 μg), R848 (0.72 μg), or vehicle control (5% dextrose) (Figure 5A). The tumor-bearing hemispheres of the brain were collected 24 h and 48 h post treatment, and TAMMs were isolated and examined with selected activation markers via flow-cytometry analysis (Figure S13). MHCII, CD86, and TNF-α were selected as M1-like/pro-inflammatory markers, as they have been shown to synergistically contribute to effective antigen presentation and immune activation, a key function of M1-like macrophages.[52] Arginase 1 (Arg1) was used to identify a subset of M2-like cells. Importantly, at both time points, GO:R848 did not affect TME leukocyte viability, confirming its biocompatibility (Figure S14A). Consistent with our *in vitro* findings, 1 day post treatment with GO:R848, TAMMs displayed a significantly increased percentage TNF-α$^+$ TAMMs compared to vehicle control, which was not significantly altered with R848 administration alone (Figure 5B). The percentage of major histocompatibility complex class II (MHCII; "M1-like" anti-tumoral and activation marker) was also significantly elevated compared to vehicle control, which coincided with significantly increased expression of CD86 and significantly lower expression of Arg1 (an "M2-like" pro-tumoral marker), although the total number of Arg1$^+$ TAMMs was not significantly different and remained low in proportion to total TAMMs (Figures 5B and 5C). Notably, 2 days post treatment, we observed that the percentage of TAMMs expressing TNF-α remained significantly elevated only in the GO:R848-treated tumors (Figure 5D), suggesting that *in vivo* administration GO:R848 may prolong the activity of R848 through its accumulation and persistence at the tumor site. We also observed that the GO:R848-treated groups had elevated monocytes and other leukocytes suggestive of a wider immune microenvironment reprogramming (Figures S14B and S14C).

To further validate our results, we performed immunohistological analysis to evaluate TAMM activation on days 1, 2, and 5 post treatment (Figure 6A). TAMMs (IBA1$^+$ cells) recruited to the injection site and internalizing the GO:R848 complex were initially a mixed population of "M2-like" (YM1$^+$/IBA1$^+$) and "M1-like" (CD86$^+$/IBA1$^+$) cells (Figures 6B and S15). Quantification of YM1$^+$/IBA1$^+$ cells showed that M2-like TAMMs were initially highly concentrated at the injection site but were significantly reduced by GO:R848 by day 2 post treatment, compared to both free R848- or vehicle-treated controls (Figures 6C, 6D, S16A, and S16B). In agreement, we observed that M1-like (CD86$^+$/IBA1$^+$) TAMMs were significantly increased throughout the tumor and injection site on day 1 and day 2 post treatment, with GO:R848 maintaining a significantly elevated CD86$^+$ populations on day 2 compared to injection with R848, consistent with the GO platform supporting prolonged immunomodulatory activity (Figures 6E, 6F, and S16C–S16E).

Since we observed that GO:R848 modulates the activation state of TAMMs in GBM, which have a dominant role in the establishment of an immunosuppressive and tumor-supportive microenvironment, we hypothesized that GO:R848 treatment may have an effect on the wider TME. Imaging mass cytometry (IMC) was performed on days 1, 2, and 5 post treatment to investigate markers associated with the TME (Figure S17A and Table S2). Noticeably, in GO:R848-treated samples, vimentin (epithelial-to-mesenchymal/aggressive GBM subtype marker), Ki67 (proliferation marker), and αSMA (smooth muscle/neoangiogenesis) were reduced on day 2 post treatment compared to controls (Figures S17B and S18–S20). This change coincided with the peak effects on TAMMs observed in the previous investigations (Figures 5 and 6). Taken together, these data indicate that, in addition to modulating TAMMs/immune microenvironment, GO:R848 administration induces more widespread changes to the TME.

Figure 5. GO:R848 complex enhances M1-like anti-tumoral TAMMs, 1 and 2 days post treatment *in vivo*

(A) Experimental schematic illustrating the design of the *in vivo* experiment. C57Bl/6 mice were implanted with 5 × 10^4 (1 μL) GL261-luc cells into the right striatum (i.c.). BLI was conducted on day 4 as a pre-treatment baseline to randomize mice to different groups. Five days following tumor inoculation, mice were treated by i.t. delivery of 5% dextrose, R848 (0.72 μg), or GO:R848 (10:4; 1.8 μg:0.72 μg) (n = 4/group).

(B) Percentage of pro-inflammatory cytokine (TNF-α) and M1 activation marker (CD86 and MHCII) positive macrophages (CD64$^+$MerTK$^+$) and corresponding geometric mean fluorescence intensity (gMFI) with representative flow-cytometry dotplots per treated group, on day 1 post treatment (day 6).

(C) Percentage of Arg1$^+$ (M2 activation marker) macrophages (CD64$^+$MerTK$^+$) and corresponding gMFI with representative flow-cytometry dotplots per treated group, on day 1 post treatment (day 6).

(D) Percentage and gMFI of pro-inflammatory cytokine (TNF-α) positive macrophages (CD64$^+$MerTK$^+$) and gMFI with representative flow-cytometry dotplots per treated group on day 2 post treatment (day 7).

Data are presented as mean ± SD. Statistical analysis by one-way ANOVA with Tukey's multiple-comparison test (*p < 0.05, **p < 0.01, ***p < 0.001; ns, not significant).

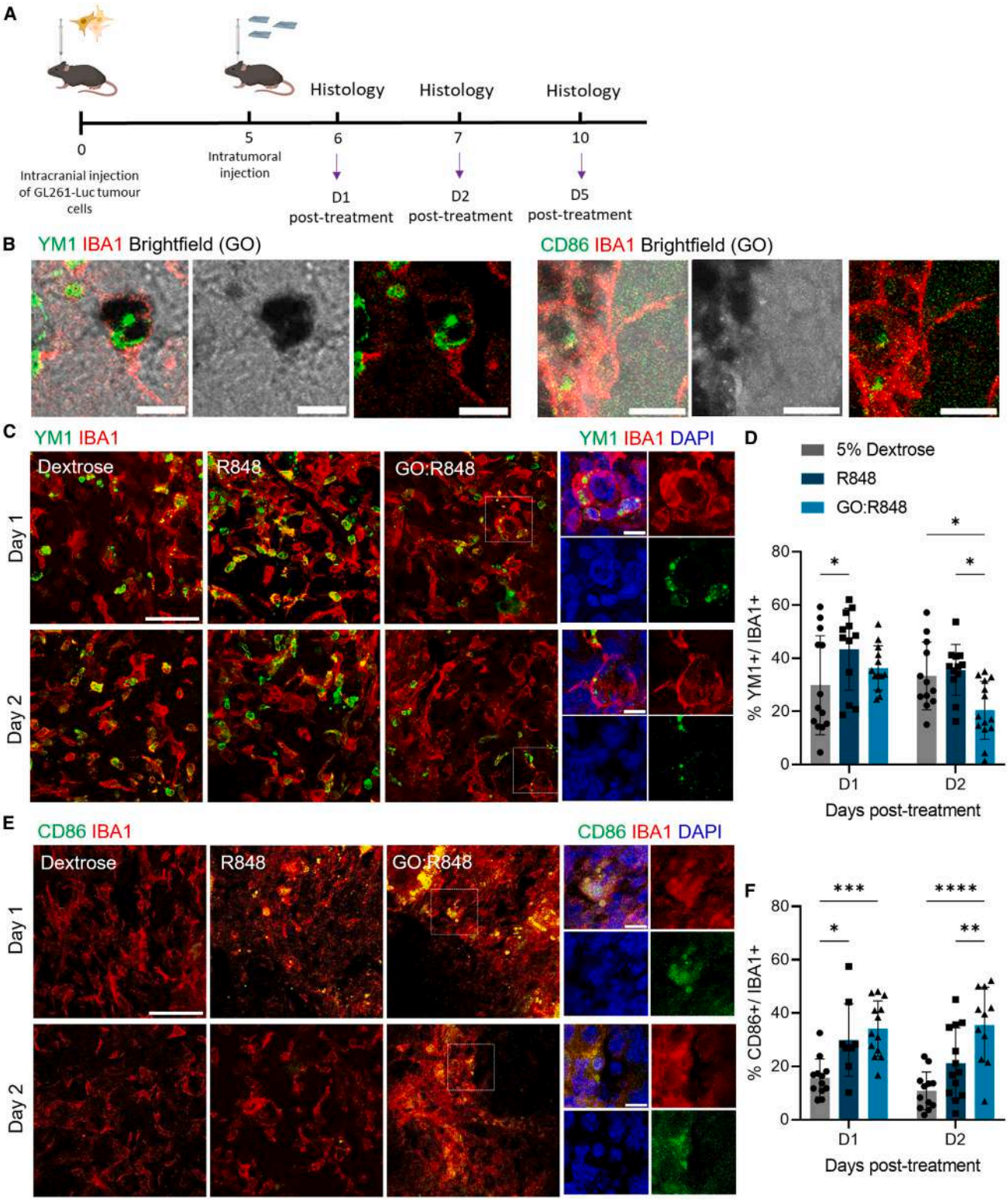

Figure 6. GO:R848 reduces "M2-like" pro-tumoral TAMMs and elevates the expression of M1-like anti-tumoral CD86⁺ TAMMs *in vivo*

(A) Schematic illustration of the experimental design.

(B) Representative high-magnification confocal images of GO:R848 (black) loaded TAMMs (red) co-expressing either YM1 or CD86 (green) in GBM tissue 24 h after injection. Scale bars, 10 μm.

(legend continued on next page)

GO:R848 treatment suppresses tumor growth in GL261 gliomas *in vivo*

Since we observed that GO:R848 treatment both modulated the polarization of TAMMs and reduced the expression of tumor progression/proliferation markers, we hypothesized that GO:R848 would affect tumor growth. Intratumoral injection of GO:R848 on day 5 and day 8 post inoculation was able to abrogate tumor growth, with mice having significantly reduced tumor volumes as measured by longitudinal bioluminescence imaging throughout the study (Figures 7A–7D and S21A). In contrast, R848 alone did not have a significant impact on tumor size, consistent with the enhanced activity of GO:R848 observed previously. The impact of GO:R848 on tumor growth was further verified by endpoint histology (Figures 7E and S21B). Importantly, no toxicity was observed with GO:R848 administration, and animal weight remained consistent between the treatment groups throughout the investigation (Figure S21C). This intratumoral administration of GO:R848 also significantly increased the recruitment of both $CD4^+$ and $CD8^+$ T cells compared to the control, indicating further immunomodulation of the TME toward a less immunologically cold microenvironment (Figure 7F). Together, these findings suggest that GO nanosheets non-covalently loaded with a TLR7/8 agonist can delay tumor progression by transiently reprogramming TAMMs and modulating the immunosuppressive microenvironment of GBM.

DISCUSSION

Tumor-associated macrophages have been shown to be highly abundant in the stroma of a variety of solid tumors, including GBM, and have been associated with poor clinical outcomes.[11,53–55] Strategies to reprogram these cells to a less-immunosuppressive, anti-tumor phenotype have been found to control or inhibit tumor progression.[28,56,57] Despite efforts to reprogram TAMMs in aggressive brain tumors such as GBM, challenges to the efficient and preferential delivery of immunomodulatory drugs to TAMMs remain.

Here, we used small, thin GO nanosheets to transport and selectively present an immunomodulatory small-molecule TLR agonist, R848, into TAMMs within the GBM TME. GO was selected because of its large surface area and ease of functionalization with bioactive agents, which presented opportunities to become a versatile and efficient drug carrier. Consistent with this, it has been demonstrated that GO can be used either systemically or locally as a delivery platform for chemotherapeutic drugs or as a vaccine-adjuvant system.[46,47] Furthermore, GO and other graphene-based materials offer additional chemical and physical attributes such as unique interactions with cells and cell components and thermal or electrical properties that can be applied therapeutically and theragnostically, including immune modulation.[58–60] While other 2D nanomaterials such as hexagonal boron nitride[61] and MXenes[59] can offer similar advantages in terms of available surface area for bioactive molecule loading, the confirmed *in vitro* and *in vivo* biocompatibility of small GO nanosheets,[42,44,62–66] as well as selective internalization within GBM TAMMs,[45] presents a compelling rationale for their application in intratumoral immunomodulation. However, the application of GO nanosheets for localized immunomodulation of the TME has not been investigated.

R848 has been previously shown to achieve M2-like macrophage to M1-like reprogramming in solid tumors such as melanoma and pancreatic cancer.[24,26,67] Although systemic administration of R848 can induce an anti-tumor responses, this has required high doses (60–200 μg) with regular repeat administration of the drug to achieve therapeutic benefit.[22,68,69] This includes when use of tumor-selective and BBB-penetrating nanocarriers have been employed.[22] In addition, systemic administration of high-dose R848 has been associated with adverse effects, including brain edema, as a result of a high degree of peripheral inflammation.[29,70,71] This has been highly limiting to the clinical translation of R848 and other TLR agonists despite initial pre-clinical successes.[30] In contrast, local administration of R848 can be used in more moderate dosages (<10 μg) with no additional toxicities, but its effects can be limited by rapid diffusion away from the site of injection or rapid metabolism of the free drug molecules. Combining R848 with a nanomaterial that is retained in the TME, such as GO, could be a strategy to increase the interaction of R848 with TAMMs and enhance its local immunomodulatory effects without potentiating off-target toxicities. Although GO and functionalized forms of GO are suitable for systemic administration, accumulation in off-target organs, urinary excretion, and minimal BBB translocation would likely be a limiting factor for effective brain tumor applications.[64,72] Instead, we exploited the advantageous biodistribution of locally administered GO in the TME of GBM[46] to passively target a small-molecule TLR7/8 agonist (R848) into these tumor myeloid cells for the purpose of local immunomodulation. Indeed, in the present work we confirmed the improved biological efficacy of GO:R848 in macrophage reprogramming both *in vitro* and *in vivo* with no evidence of toxicity.

Consistent with previous studies using bare GO sheets[45] or GO chemotherapy complexes,[46] we observed that GO:R848 spontaneously redistributed throughout the tumor without penetrating the surrounding non-tumoral brain tissue. The selective internalization by TAMMs, along with their known propensity for tumor infiltration and persistence,[11] likely contributes to this

(C) Representative confocal images of $IBA1^+$ TAMMs (red) and $YM1^+$ M2-like pro-tumoral TAMMs (green) on day 1 and day 2 post treatment with 5% dextrose, R848 (0.72 μg), or GO:R848 (10:4; 1.8 μg:0.72 μg). Scale bar, 50 μm.

(D) Percentage of $YM1^+IBA1^+$ cells out of the total $IBA1^+$ population of cells on days 1 and 2 post treatment with 5% dextrose, R848, or GO:R848. $n = 3$ mice/group, 4–5 fields of view/mouse.

(E) Representative confocal images of $IBA1^+$ TAMMs (red) and $CD86^+$ M1-like TAMMs (green) on days 1 and 2 post treatment with 5% dextrose, R848 (0.72 μg), or GO:R848 (10:4; 1.8 μg:0.72 μg). Scale bar, 50 μm.

(F) Percentage of $CD86^+IBA1^+$ cells out of the total $IBA1^+$ cell population on days 1 and 2 post treatment. $n = 3$ mice/group, 4–5 fields of view/mouse.

Data are presented as mean ± SD. Statistical analysis by two-way ANOVA with Tukey's multiple-comparison test (*$p < 0.05$, **$p < 0.01$, ***$p < 0.001$, ****$p < 0.0001$).

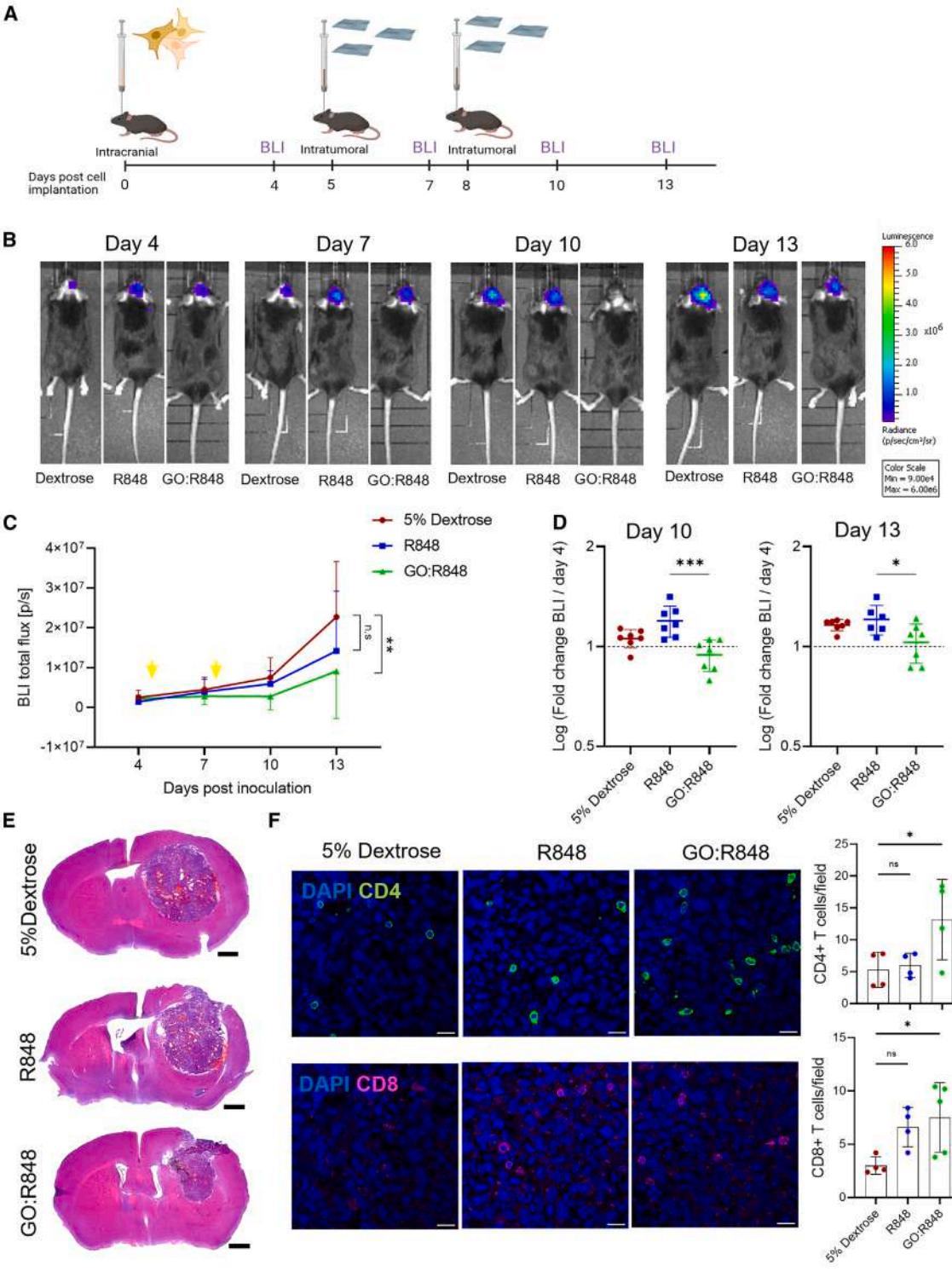

Figure 7. GO:R848 alters the GBM microenvironment and inhibits tumor growth

(A) C57Bl/6 mice were implanted with 5 × 10^4 (1 μL) GL261-luc cells into the right striatum (i.c.). BLI was conducted on day 4 as a pre-treatment baseline to normalize mice to different groups. Five days and 8 days following tumor inoculation, mice were treated by i.t. delivery of 5% dextrose, free R848, or GO:R848 (10:4). Tumor growth was monitored via BLI on days 7, 10, and 13 post tumor inoculation.

(B) Representative BLI images from individual mice per group.

(legend continued on next page)

identified retention of GO within the TME and the prolonged effects of the delivered R848. Additionally, prior research has shown that macrophages, including brain-resident microglia, can support the degradation GO *in vivo*.[63,64] Indeed, evaluating the long-term persistence, degradation, and clearance of intratumorally administered graphene materials will be crucial for confirming the safety of such strategies for clinical translation.

In addition to the direct effects of GO:R848 on macrophages and microglia, we also observed that this immunomodulatory nanocomplex was able to alter the wider GBM microenvironment and inhibit tumor progression. Further work is warranted to confirm the mechanisms by which GO:R848-mediated immunomodulation alters the proliferative, angiogenic, and aggressive nature of the tumor, although this is likely due to a combination of reduced tumor-supportive actions of M2-like cells (release of angiogenic factors, mitogens, extracellular matrix remodeling) and increased tumor-destructive actions of M1-like cells (release of cytotoxic cytokines, phagocytosis, inflammatory cascades).[11] Our data further corroborate recent findings that intratumoral activation of TLR7/8 can increase peripheral lymphocyte infiltration into the tumor and inhibit tumor growth.[22,25,73,74] The immunosuppressive microenvironment and paucity of tumor-reactive lymphocytes has been identified as a limiting factor to the efficacy of immunotherapies. Current clinically used immunotherapies such as cancer vaccines, checkpoint inhibitors, and chimeric antigen receptor (CAR) T cells have demonstrated little or no efficacy for high-grade gliomas.[75] For instance, the PD-1 checkpoint inhibitor nivolumab failed to show any significant benefit in patient survival,[76,77] and cancer vaccines designed to induce anti-tumor-specific $CD8^+$ T cell responses were not successful in late-stage clinical trials.[78] Given the significant role played by TAMMs in immunosuppression through secretion of cytokines, suppression of co-activation factors, or expression of checkpoint molecules,[79–81] all contributing to inducing T cell anergy/exhaustion,[82,83] the effective reprogramming of TAMMs to a less-immunosuppressive state may enhance the actions of systemic immunotherapies. Thus, a combination of nanomaterial-mediated local immunomodulation with existing systemic immunotherapies could solve the issue of immune-surveillance escape and low efficacy. Further studies are required to evaluate whether the GO:R848 platform presented here could provide additional synergistic effects in combination with systemic immunotherapies along with additional validation in other human GBM-relevant models to enhance translatability.[84]

In this study, we have demonstrated that GO nanosheets can provide a suitable nanomaterial platform to effectively enhance the reprogramming of M2-like macrophages/microglia to M1-like macrophages/microglia both *in vitro* and *in vivo*. Direct intratumoral administration of GO:R848 complexes offered effective modulation of the overall GBM TME, resulting in tumor-growth inhibition in this highly aggressive brain cancer model. These findings highlight the potential of graphene-based immunomodulatory flat nanoconstructs as possible combinatorial treatment modalities to engineer an immunologically "hotter" TME that could be adapted to enhance other systemic cancer therapies, such as checkpoint inhibitors or cancer vaccines.

EXPERIMENTAL PROCEDURES

Reagents

Resiquimod (TLR7/8 agonist) was purchased from Invivogen (France) and prepared following the manufacturer's instructions. Graphene oxide (GO) was synthesized and characterized at the Nanomedicine Group of the Catalan Institute of Nanoscience and Nanotechnology (ICN2) using a modified Hummers' method as previously described.[85] The nanomaterials used in this study were confirmed endotoxin free. Cell-culture reagents and chemicals were purchased from Sigma-Aldrich (Merck, UK) unless otherwise stated.

Preparation of non-covalent GO:R848 complexes

GO was neutralized at pH 10 using NaOH and R848 was added, previously reconstituted in water for injection, at the mass ratio GO:R848 of 10:4 for the *in vivo* experiments and 10:0.01 mass ratio for the *in vitro* experiments (GO concentration of 1 mg/mL). The mixture was incubated for 30 min, at room temperature (RT) in an orbital shaker at 1 RCF and then incubated for a further 1 h at RT without shaking. For the *in vitro* experiments, 50 μL of complex was mixed in 950 μL of BMDM culture medium. For the *in vivo* experiments, complex was resuspended in 5% dextrose (Sigma, UK) at a final dose of 0.6 μg/μL GO/0.24 μg/μL R848 up to 24 h prior to injection.

Physicochemical characterization of GO and GO:R848 complexes

For AFM, mica surface (Ted Pella) cleaved with poly-L-lysine solution (Sigma-Aldrich) was used for the deposition of GO and GO:R848 samples at GO concentrations of 100 μg/mL. The images were recorded in 5 μm × 5 μm dimensions, in air-tapping mode with the atomic force microscope Asylum MFP-3D (Oxford Instruments) at the ICN2 Advanced Electronic Materials and Devices Group. Silicon probes (Ted Pella) were selected with 40 N/m nominal force and 300 kHz resonance frequency. The processing was performed with Gwyddion (version 2.57) and Origin (version b9.5.0.193) software.

For SEM, GO and GO:R848 samples, at GO concentrations of 100 μg/mL, were deposited on the Lacey C grid (Ted Pella). The images were recorded at the ICN2 Electron Microscopy Unit using a Magellan 400L field-emission microscope (Oxford Instruments) coupled with a secondary electrons detector Everhart-Thornley. The conditions used were 20 kV acceleration voltage and 100 pA beam current. Finally, the image was processed with ImageJ software (version 1.8.0) for size-distribution analysis.

Colloidal stability studies were performed at the ICN2 Molecular Spectroscopy and Optical Microscopy Facility with a Zetasizer Nano ZS (Malvern Instruments). GO and GO:R848 samples, at GO concentrations of 20 μg/mL, filled the capillary cells and were measured three times at RT by applying the water viscosity and refractive index. Data analysis was carried out with Zetasizer (version 7.12) and Origin (version b9.5.0.193) software. Data were expressed as mean ± standard deviation.

(C) Tumor growth presented as the mean total flux (p/s) based on bioluminescence signal per group after treatment (yellow arrows) with 5% dextrose, free R848, or GO:R848 (3 μL/injection). n = 7/group. Statistical analysis by two-way ANOVA with Tukey's multiple-comparison test (**$p < 0.01$; ns, not significant).
(D) Log(fold change in BLI signal vs. baseline) on days 10 and 13 post inoculation. Baseline (day 4) is represented by dotted line. One-way ANOVA with Tukey's multiple-comparison test (*$p < 0.05$, ***$p < 0.001$).
(E) Representative H&E-stained sections on day 14 post tumor implantation, after administration of 5% dextrose, R848, and GO:R848. Scale bars, 1,000 μm.
(F) Representative confocal images of $CD4^+$ T cells (green) and $CD8^+$ T cells (magenta) with nuclei/DAPI (blue), 14 days post tumor inoculation and after treatment with 5% dextrose, R848 (0.72 μg), or GO:R848 (10:4; 1.8 μg:0.72 μg). Scale bars, 20 μm. Quantification of $CD4^+$ or $CD8^+$ T cells per field. n = 4 mice/group. Statistical analysis by one-way ANOVA with Tukey's multiple-comparison test (*$p < 0.05$; ns, not significant).
All data are presented as mean ± SD.

Additional information is presented in the supplemental experimental procedures.

Bone-marrow-derived macrophage isolation and maturation

BMDMs were isolated by flushing the bone marrow from fibulas and tibias of C57BL/6 mice with DMEM complemented with 1% L-glutamine, 1% penicillin/streptomycin, and 10% fetal bovine serum (FBS). Bone-marrow cells were centrifuged at 300 × *g* for 5 min at RT. Pellet was resuspended in medium with 10 ng/mL murine colony-stimulating factor (M-CSF, PeproTech, USA) and were passed through a 100-μm strainer to remove any bone fractions. Bone-marrow cells were cultured in T25 flasks (Corning, UK), with 5% CO_2 at 37°C. For maturation, medium was changed every other day with complete medium complemented with M-CSF with a final concentration of 10 ng/mL up to day 6, when maturation of macrophages was tested using flow cytometry and/or used for the subsequent experiments.

In vitro activation assay

Macrophage activation was determined by flow cytometry. BMDMs were seeded at a density of 150K cells per well in a non-treated 24-well plate (Corning) and treated for 24 h with the different treatments. Supernatant was then collected for ELISA, and cells were detached with 10 mM EDTA for 15 min at 4°C. EDTA was neutralized with equal volume of BMDM medium. Cells were then centrifuged at 300 × *g* for 5 min at RT and resuspended in 100 μL of PBS. Finally, cells were transferred to a 96-well V-bottom plate for staining and flow-cytometry analysis.

Flow-cytometry analysis of BMDMs

BMDMs were harvested and washed with PBS by centrifugation at 300 × *g* for 5 min at 8°C. 45 μL of Zombie UV live/dead staining (BioLegend, USA) was applied after 1:2,000 dilution with PBS, and the plate was incubated in darkness at RT for 15 min. The plate was recentrifuged at the same speed and supernatant discarded, and cells were incubated with the conjugated primary antibody (F4/80, CD80, CD206, and CD11b) and Fc receptor blocker for 1 h at 4°C in darkness. Following incubation, the plate was centrifuged at 300 × *g* for 5 min at 8°C. Two washing steps were conducted, and cells were fixed with 1% paraformaldehyde (PFA) for 10 min at RT, following by two additional washing steps with flow buffer. Finally, the cells were resuspended in 200 μL of flow buffer and stored in darkness at 4°C until flow cytometry. Flow cytometry was performed using the MCCIR FCF BD LSRFortessa cytometer (BD Bioscience, UK).

Phagocytosis assay with beads

BMDMs were plated in non-treated 24-well plates at a density of 200K cells/well and were treated for 24 h with GO:R848 or controls, as mentioned above. FACS-based phagocytosis assays were performed to evaluate the phagocytic ability of macrophages toward green-fluorescent beads. Following BMDM treatment, cells were washed once with PBS (Sigma) and incubated with 1-μm green-fluorescent beads (Invitrogen, UK) for 1 h with 5% CO_2 at 37°C. Macrophages were harvested post treatments, divided into 96-well rounded low-attachment plates (Corning), and processed as mentioned above for flow cytometry.

Optical microscopy

Cells were imaged using a PrimoVert microscope (Zeiss) with a Primo Plan Achromat 10×/0.25 Ph1 lens. Images were captured via an AxioCam ERc5s camera with ZEN light software. All conditions were kept consistent throughout the imaging process.

Glioblastoma cell lines and culture

The murine GL261 glioblastoma cell line was obtained from the Leibniz Institute DSMZ (Germany). The murine GL261-luc (modified to express luciferase) cell line was kindly provided by Prof. Brian Bigger (The University of Manchester, UK). GL261 cell lines were cultured in T-75 cell-culture flasks (Corning) and maintained in RPMI 1640 medium with L-glutamine and sodium bicarbonate supplemented with 10% FBS and 1% penicillin/streptomycin at 37°C in a humidified atmosphere containing 5% CO_2.

Animals

All animal experiments were performed at the University of Manchester in accordance with the Animals (Scientific Procedures) Act 1986 (UK), approved by the University of Manchester Ethical Review Committee and under a UK Home Office Project License P089E2E0A. Animals were housed in groups of 4–5 within ventilated cages with *ad libitum* access to food and water. Female C57BL/6 (Envigo, UK) mice, 8–12 weeks old, were allowed to acclimatize to the facility for at least 1 week prior to any procedure.

Intracranial inoculation of glioma cells

Female C57BL/6 mice (8–9 weeks old) were anesthetized using isoflurane (2.5% induction and 1.8%–2% maintenance in medical oxygen at a rate of 1.5–2 L min^{-1}) and placed on a stereotactic frame. Prior to surgery, animals received 0.1 mg/kg buprenorphine (Buprenex, Reckitt Benckiser, UK). A midline incision was performed to expose the cranium, skull was dried, and a 0.7-mm bore hole was drilled (Fine Science Tools, Canada) above the right striatum at 0.0 mm anterior and 2.3 mm lateral from bregma. A 10-μL Hamilton syringe (SYR10, Hamilton, USA) with a 26-gauge blunt needle (Hamilton) was lowered to 3 mm below the cortical surface and slowly withdrawn 0.6 mm to create a pocket, with a final injection point at 2.4-mm depth. 5 × 10^4 GL261 or GL261-luc cells in 1 μL of PBS were injected slowly over 5 min at a rate of 0.2 μL/min. Post injection, the needle was kept in place for 3 min to minimize reflux and slowly withdrawn to minimize any innate injury. The skin incision was closed with 6-0 coated Vicryl sutures (Ethicon, UK), and animals were allowed to recover in a heated environment.

Intratumoral injection

Mice underwent intratumoral injection with 3 μL of 5% dextrose, free R848, or GO:R848 in 5% dextrose on day 5 post tumor cell implantation. Mice were anesthetized and prepared for stereotactic surgery as described above. The original incision was reopened, and a 33-gauge needle connected to a 10 μL Hamilton Neuros syringe was passed through the original bore hole to a depth of 2.2 mm to ensure the targeting of the tumor center. 3 μL of GO:R848 complex or controls was injected over 15 min (0.2 μL/min). Post injection, the needle was kept in place for 3 min to minimize reflux and slowly withdrawn over 1–3 min. The skin incision was closed with 6-0 coated Vicryl sutures, and animals were allowed to recover in a heated environment and provided with mash food. For the second intratumoral injection the same process was followed, with the needle lowered to a depth of 2 mm, assuming that tumor (day 8) grew evenly.

In vivo bioluminescence imaging

Tumor-bearing mice were anesthetized with 2% isoflurane (1.5% maintenance in medical oxygen) followed by intraperitoneal injection of 150 mg/kg mouse D-luciferin (15 mg/mL; Promega, UK) in PBS. Eight minutes post injection, bioluminescence signals were detected using sequential imaging (15 measurements at 2-min intervals) with an *in vivo* imaging system (IVIS Lumina II, PerkinElmer, UK). Images were analyzed with Living Image software (version 4.7) (PerkinElmer), and results were plotted in GraphPad Prism software (version 6.01).

Postmortem tissue processing

At the end of each experiment, tumor-bearing mice were anesthetized with 2.5% isoflurane and culled by cardiac perfusion with 20 mL of 2 mM EDTA in PBS. Brains were removed and fixed overnight at 4°C in 4% PFA in PBS buffer for 24 h and later placed in 30% sucrose in PBS for at least 24 h to ensure cryopreservation. The brains were snap frozen in cold isopentane (−40°C to −50°C), and coronal sections (20 μm thickness) were taken using a cryostat (Leica CM1950, Leica Biosystems, Germany).

Analysis of tumor-infiltrating immune cells by flow cytometry

Following perfusion, tumor-bearing hemispheres were minced in a non-culture-treated 12-well plate (Corning), and 1 mL of Accutase (Sigma-Aldrich, UK) was added to each sample before being incubated at 37°C for 25 min. The digested tissue was then passed through a 100-μm strainer with the help of flow buffer (PBS + 2 mM EDTA, 2% FBS) and was centrifuged at 300 × *g* for 7 min at 8°C. Pellets were then resuspended in 6 mL of 35% Percoll

(Sigma-Aldrich, UK), samples were spiked with 2 mL of 70% Percoll (Sigma-Aldrich) at the bottom of a 35% Percoll layer by a 19-gauge needle, and 1 mL of PBS was added on the top, creating three clearly visible layers. Following centrifugation at 650 × *g* for 15 min at 20°C (acceleration 4/deceleration 1), the top fat layer was removed, and the transparent layer was isolated. The cells were then washed with flow buffer and centrifuged at 300 × *g* for 7 min at 8°C. The medium was aspirated and cells resuspended in 1 mL of flow buffer ready for cell counting. Samples in suspension were recentrifuged, 300 × *g* at 8°C, for 5 min. The cell pellet was then resuspended to 1 × 10^6 cells/200 μL flow buffer, which was then transferred to a 96-well V-bottom plate (ThermoFisher, UK). The plate was centrifuged at 300 × *g* for 5 min at 8°C and supernatant was removed. 10 μL of Zombie UV (1:2,000) live/dead staining (BioLegend) was applied, and the plate was incubated in darkness at RT for 15 min. Conjugated antibodies were added (Table S3), and the plate was then incubated for 30 min at 4°C in darkness. Two washing steps were conducted by removal of the supernatant, addition of 50 μL of flow buffer, and centrifugation at 500 × *g* for 3 min at 8°C. Fixation with 1% PFA for 10 min at RT was performed, followed by two washing steps with flow buffer. Finally the supernatant was removed, and cells were resuspended in 100 μL of flow buffer and stored in darkness at 4°C until flow cytometry. Fluorescence was detected using the MCCIR FCF BD LSRFortessa cytometer (BD Bioscience), and data were analyzed via FlowJo (version 10.6.1). Fluorescence minus one (FMO) controls were applied for antibodies (anti-CX3CR1, anti-MerTK, anti-F4/80, anti-SiglecH, anti-MHCII, anti-TNFα, anti-CD86, anti-Arg1, anti-CD3, anti-CD19, anti-NK1.1, and anti-TCRb) for the purpose of gating.

H&E staining

Sections were stained with H&E to observe the histological characteristics of the tumor sections and determine the tumor volume. Cryosections were left for 10 min at RT to dry, and staining was performed as previously described.[46] The whole staining process was performed automatically by Leica autostainer (Leica Biosystems, Germany). Slides were scanned using a 3D Histech Panoramic 250 slide scanner and analyzed using CaseViewer software (2.4.0.119028).

Immunofluorescence

Cryosections were removed from the freezer and allowed to thaw prior to being post-fixed in ice-cold acetone for 10 min and permeabilized in 0.3% Triton X-100 (Sigma-Aldrich) solution. Sections were then incubated with blocking buffer composed of 5F% (v/v) normal donkey serum (Sigma-Aldrich) and 1% BSA (Sigma-Aldrich) in PBS-Triton X-100 0.2% for 1.5 h at RT. Diluted primary antibodies were added onto sections and incubated in a humidified chamber at 4°C overnight. Sections were then washed three times with washing buffer (0.2% Triton X-100 in PBS) and incubated with diluted secondary antibodies for 1 h at RT. After six more washing steps with the washing buffer, 1× PBS, and distilled water, sections were mounted with Prolong Gold Antifade medium containing DAPI and let dry at RT overnight in darkness. Fluorescence microscopy images were acquired by a Leica TCS SP8 AOBS inverted confocal microscope using the 63× objective with optical Z spacing as specified by the LASX imaging software (Leica, UK). The antibodies used in these investigations are given in Table S4.

Imaging analysis

Images were analyzed and quantified using ImageJ (NIH, USA). Z-stack images separated to different channels, and each marker was normalized based on the negative control (only secondary antibody). $IBA1^+$ cells were manually counted via cell counter per field of view and were co-localized with CD86 or YM1 channels. Individual $CD86^+$ or $YM1^+$ cells were counted using the cell counter function, and the percentage of double-positive cells was calculated out of the total $IBA1^+$/field of view.

Imaging mass cytometry: Staining, data acquisition, and analysis

Cryosections of thickness 10 μm were allowed to thaw prior to being post-fixed in ice-cold acetone for 10 min. Sections were incubated for 10 min in warm sodium citrate buffer for antigen retrieval, and buffer was allowed to cool down to RT before being permeabilized in 0.3% Triton X-100 (Sigma) PBS solution. Sections were then incubated in 3% BSA (Sigma) in PBS for 1.5 h at RT. Metal-conjugated antibodies were diluted in 0.5% BSA, added onto sections, and incubated in a humidified chamber at 4°C (Table S2). Sections were washed three more times with the washing buffer and incubated with iridium (Fluidigm, USA) at a 1:500 dilution factor in PBS to stain the DNA. After three more washing steps, sections were allowed to dry at RT and stored at RT until tissue ablation and IMC acquisition.

The areas of acquisition were chosen based on the distinct area of the tumor, and the regions of interest (ROIs) were selected to ablate for each brain section. Prior to acquisition, the Hyperion mass cytometry system was autotuned using a 3-element tuning slide according to the provider's protocol. As an extra verification point for successful tuning, a detection of at least 500 mean duals of 175 Lu was used. The slides with sections stained with the IMC panel containing 12 metal-conjugated antibodies (Table S2) were placed in the Hyperion (Fluidigm) one by one using the same laser power. The chosen ROIs were ablated and acquired at 200 Hz. Data were exported as MCD files and visualized using the Fluidigm MCD viewer software. For data analysis, an MCD viewer was used to set minimum and maximum threshold for each image based on the unstained control. All thresholds were kept the same for each marker across the different ROIs. Merged images were composed using ImageJ software (NIH).

Statistical analysis

Data analysis and graphical design were performed using GraphPad Prism software (version 6.01). Flow-cytometry data analysis was completed using FlowJo (version 10.6.1). *p* values were calculated using two-way or one-way ANOVA with Tukey's post hoc test for multiple comparisons unless stated otherwise in figure legends. *p* values of <0.05 were considered statistically significant. Data were plotted as mean ± SD unless stated otherwise.

RESOURCE AVAILABILITY

Lead contact

Further information and requests for resources and reagents should be directed to and will be fulfilled by the lead contact, Kostas Kostarelos (kostas.kostarelos@manchester.ac.uk).

Materials availability

The new materials described in this study (GO:R848 complexes) can be synthesized following the detailed experimental methods provided herein.

Data and code availability

The data that support the findings of this study are available in the supplemental information of this article. This paper does not report original code.

ACKNOWLEDGMENTS

M.S., T.K., A.T., K.A., H.P., A.S.M., and K.K. would like to acknowledge the United Kingdom Research and Innovation (UKRI) Engineering and Physical Sciences Research Council (EPSRC) 2D-Health Programme Grant (EP/P00119X/1) for financial support. T.K. and K.K. would also like to acknowledge the UKRI (EPSRC) for an International Centre-to-Centre grant (EP/S030719/1). The ICN2 is funded by the CERCA programme, Generalitat de Catalunya and is supported by the Severo Ochoa Centres of Excellence program by the Spanish Research Agency (AEI, grant no. SEV-2017-0706). The authors would like to acknowledge the ICN2 Advanced Electronic Materials and Devices Group (Prof. Jose A. Garrido) for access to the AFM instrumentation. The authors would like to thank Kate Hills and Abbie Dodd for their assistance with surgeries and sample processing. The authors would also like to thank the Bioimaging core facility, Biological Services facility, Flow Cytometry facility, and Histology core facility at the University of Manchester for technical support and access to equipment.

AUTHOR CONTRIBUTIONS

M.S., T.K., and K.K. initiated and designed the research. K.K. and T.K. coordinated and supervised the research. M.S. and T.K. conducted *in vivo* and *in vitro* experiments and data analysis. A.T. and K.A. assisted with *in vivo*

experiments, *in vivo* imaging, and tissue processing. D.D. and N.L. developed the complexation protocol, and D.D. performed the complex characterization. A.S.M. and H.P. advised in experimental design and interpretation of data. M.S., T.K., D.D., N.L., A.S.M., and K.K. contributed to the writing of the manuscript.

DECLARATION OF INTERESTS

K.K. is a member of the advisory board of *Cell Reports Physical Science*; however, this did not influence editorial consideration of the manuscript.

SUPPLEMENTAL INFORMATION

Supplemental information can be found online at https://doi.org/10.1016/j.xcrp.2024.102342.

Received: May 13, 2024
Revised: September 22, 2024
Accepted: November 22, 2024
Published: December 18, 2024

REFERENCES

1. Komotar, R.J., Otten, M.L., Moise, G., and Connolly, E.S., Jr. (2008). Radiotherapy plus concomitant and adjuvant temozolomide for glioblastoma-a critical review. Clin. Med. Oncol. *2*, 421–422. https://doi.org/10.4137/cmo.s390.
2. Hanif, F., Muzaffar, K., Perveen, K., Malhi, S.M., and Simjee, S.U. (2017). Glioblastoma multiforme: A review of its epidemiology and pathogenesis through clinical presentation and treatment. Asian Pac. J. Cancer Prev. APJCP *18*, 3–9. https://doi.org/10.22034/APJCP.2017.18.1.3.
3. Louis, D.N., Perry, A., Wesseling, P., Brat, D.J., Cree, I.A., Figarella-Branger, D., Hawkins, C., Ng, H.K., Pfister, S.M., Reifenberger, G., et al. (2021). The 2021 WHO classification of tumors of the central nervous system: A summary. Neuro Oncol. *23*, 1231–1251. https://doi.org/10.1093/neuonc/noab106.
4. Landry, A.P., Balas, M., Alli, S., Spears, J., and Zador, Z. (2020). Distinct regional ontogeny and activation of tumor associated macrophages in human glioblastoma. Sci. Rep. *10*, 19542. https://doi.org/10.1038/s41598-020-76657-3.
5. Belgiovine, C., D'Incalci, M., Allavena, P., and Frapolli, R. (2016). Tumor-associated macrophages and anti-tumor therapies: complex links. Cell. Mol. Life Sci. *73*, 2411–2424. https://doi.org/10.1007/s00018-016-2166-5.
6. Mantovani, A., and Locati, M. (2013). Tumor-associated macrophages as a paradigm of macrophage plasticity, diversity, and polarization: lessons and open questions. Arterioscler. Thromb. Vasc. Biol. *33*, 1478–1483. https://doi.org/10.1161/ATVBAHA.113.30016.
7. Solinas, G., Germano, G., Mantovani, A., and Allavena, P. (2009). Tumor-associated macrophages (TAM) as major players of the cancer-related inflammation. J. Leukoc. Biol. *86*, 1065–1073. https://doi.org/10.1189/jlb.0609385.
8. Gordon, S. (2003). Alternative activation of macrophages. Nat. Rev. Immunol. *3*, 23–35. https://doi.org/10.1038/nri978.
9. Kim, H.-J., Park, J.H., Kim, H.C., Kim, C.W., Kang, I., and Lee, H.K. (2022). Blood monocyte-derived CD169^{+} macrophages contribute to antitumor immunity against glioblastoma. Nat. Commun. *13*, 6211. https://doi.org/10.1038/s41467-022-34001-5.
10. Li, W., and Graeber, M.B. (2012). The molecular profile of microglia under the influence of glioma. Neuro Oncol. *14*, 958–978. https://doi.org/10.1093/neuonc/nos116.
11. Hambardzumyan, D., Gutmann, D.H., and Kettenmann, H. (2016). The role of microglia and macrophages in glioma maintenance and progression. Nat. Neurosci. *19*, 20–27. https://doi.org/10.1038/nn.4185.
12. Basheer, A.S., Abas, F., Othman, I., and Naidu, R. (2021). Role of inflammatory mediators, macrophages, and neutrophils in glioma maintenance and progression: Mechanistic understanding and potential therapeutic applications. Cancers *13*, 4226. https://doi.org/10.3390/cancers13164226.
13. Zhang, M., Hutter, G., Kahn, S.A., Azad, T.D., Gholamin, S., Xu, C.Y., Liu, J., Achrol, A.S., Richard, C., Sommerkamp, P., et al. (2016). Anti-CD47 treatment stimulates phagocytosis of glioblastoma by M1 and M2 polarized macrophages and promotes M1 polarized macrophages in vivo. PLoS One *11*, e0153550. https://doi.org/10.1371/journal.pone.0153550.
14. Poli, A., Wang, J., Domingues, O., Planagumà, J., Yan, T., Rygh, C.B., Skaftnesmo, K.O., Thorsen, F., McCormack, E., Hentges, F., et al. (2013). Targeting glioblastoma with NK cells and mAb against NG2/CSPG4 prolongs animal survival. Oncotarget *4*, 1527–1546. https://doi.org/10.18632/oncotarget.1291.
15. Huang, L., Xu, H., and Peng, G. (2018). TLR-mediated metabolic reprogramming in the tumor microenvironment: potential novel strategies for cancer immunotherapy. Cell. Mol. Immunol. *15*, 428–437. https://doi.org/10.1038/cmi.2018.4.
16. Feng, M., Chen, J.Y., Weissman-Tsukamoto, R., Volkmer, J.P., Ho, P.Y., McKenna, K.M., Cheshier, S., Zhang, M., Guo, N., Gip, P., et al. (2015). Macrophages eat cancer cells using their own calreticulin as a guide: roles of TLR and Btk. Proc. Natl. Acad. Sci. USA *112*, 2145–2150. https://doi.org/10.1073/pnas.1424907112.
17. Hemmi, H., Kaisho, T., Takeuchi, O., Sato, S., Sanjo, H., Hoshino, K., Horiuchi, T., Tomizawa, H., Takeda, K., and Akira, S. (2002). Small anti-viral compounds activate immune cells via the TLR7 MyD88–dependent signaling pathway. Nat. Immunol. *3*, 196–200. https://doi.org/10.1038/ni758.
18. Tambunlertchai, S., Geary, S.M., and Salem, A.K. (2022). Topically applied resiquimod versus imiquimod as a potential adjuvant in melanoma treatment. Pharmaceutics *14*, 2076. https://doi.org/10.3390/pharmaceutics14102076.
19. Stathopoulos, A., Pretto, C., Devillers, L., Pierre, D., Hofman, F.M., Kruse, C., Jadus, M., Chen, T.C., and Schijns, V.E.J.C. (2012). Development of immune memory to glial brain tumors after tumor regression induced by immunotherapeutic toll-like receptor 7/8 activation. OncoImmunology *1*, 298–305. https://doi.org/10.4161/onci.19068.
20. Chirasani, S.R., Leukel, P., Gottfried, E., Hochrein, J., Stadler, K., Neumann, B., Oefner, P.J., Gronwald, W., Bogdahn, U., Hau, P., et al. (2013). Diclofenac inhibits lactate formation and efficiently counteracts local immune suppression in a murine glioma model. Int. J. Cancer *132*, 843–853. https://doi.org/10.1002/ijc.27712.
21. Grauer, O.M., Molling, J.W., Bennink, E., Toonen, L.W.J., Sutmuller, R.P.M., Nierkens, S., and Adema, G.J. (2008). TLR ligands in the local treatment of established intracerebral murine gliomas. J. Immunol. *181*, 6720–6729. https://doi.org/10.4049/jimmunol.181.10.6720.
22. Turco, V., Pfleiderer, K., Hunger, J., Horvat, N.K., Karimian-Jazi, K., Schregel, K., Fischer, M., Brugnara, G., Jähne, K., Sturm, V., et al. (2023). T cell-independent eradication of experimental glioma by intravenous TLR7/8-agonist-loaded nanoparticles. Nat. Commun. *14*, 771. https://doi.org/10.1038/s41467-023-36321-6.
23. Morse, M.A., Chapman, R., Powderly, J., Blackwell, K., Keler, T., Green, J., Riggs, R., He, L.-Z., Ramakrishna, V., Vitale, L., et al. (2011). Phase I study utilizing a novel antigen-presenting cell-targeted vaccine with Toll-like receptor stimulation to induce immunity to self-antigens in cancer patients. Clin. Cancer Res. *17*, 4844–4853. https://doi.org/10.1158/1078-0432.CCR-11-0891.
24. Singh, M., Khong, H., Dai, Z., Huang, X.-F., Wargo, J.A., Cooper, Z.A., Vasilakos, J.P., Hwu, P., and Overwijk, W.W. (2014). Effective innate and adaptive antimelanoma immunity through localized TLR7/8 activation. J. Immunol. *193*, 4722–4731. https://doi.org/10.4049/jimmunol.1401160.

25. Rodell, C.B., Arlauckas, S.P., Cuccarese, M.F., Garris, C.S., Li, R., Ahmed, M.S., Kohler, R.H., Pittet, M.J., and Weissleder, R. (2018). TLR7/8-agonist-loaded nanoparticles promote the polarization of tumour-associated macrophages to enhance cancer immunotherapy. Nat. Biomed. Eng. *2*, 578–588. https://doi.org/10.1038/s41551-018-0236-8.

26. Anfray, C., Mainini, F., Digifico, E., Maeda, A., Sironi, M., Erreni, M., Anselmo, A., Ummarino, A., Gandoy, S., Expósito, F., et al. (2021). Intratumoral combination therapy with poly(I:C) and resiquimod synergistically triggers tumor-associated macrophages for effective systemic antitumoral immunity. J. Immunother. Cancer *9*, e002408. https://doi.org/10.1136/jitc-2021-002408.

27. Ursu, R., Carpentier, A., Metellus, P., Lubrano, V., Laigle-Donadey, F., Capelle, L., Guyotat, J., Langlois, O., Bauchet, L., Desseaux, K., et al. (2017). Intracerebral injection of CpG oligonucleotide for patients with de novo glioblastoma-A phase II multicentric, randomised study. Eur. J. Cancer *73*, 30–37. https://doi.org/10.1016/j.ejca.2016.12.003.

28. Pyonteck, S.M., Akkari, L., Schuhmacher, A.J., Bowman, R.L., Sevenich, L., Quail, D.F., Olson, O.C., Quick, M.L., Huse, J.T., Teijeiro, V., et al. (2013). CSF-1R inhibition alters macrophage polarization and blocks glioma progression. Nat. Med. *19*, 1264–1272. https://doi.org/10.1038/nm.3337.

29. Dudek, A.Z., Yunis, C., Harrison, L.I., Kumar, S., Hawkinson, R., Cooley, S., Vasilakos, J.P., Gorski, K.S., and Miller, J.S. (2007). First in human phase I trial of 852A, a novel systemic toll-like receptor 7 agonist, to activate innate immune responses in patients with advanced cancer. Clin. Cancer Res. *13*, 7119–7125. https://doi.org/10.1158/1078-0432.CCR-07-1443.

30. Yang, Y., Li, H., Fotopoulou, C., Cunnea, P., and Zhao, X. (2022). Toll-like receptor-targeted anti-tumor therapies: Advances and challenges. Front. Immunol. *13*, 1049340. https://doi.org/10.3389/fimmu.2022.1049340.

31. Carpentier, A., Metellus, P., Ursu, R., Zohar, S., Lafitte, F., Barrié, M., Meng, Y., Richard, M., Parizot, C., Laigle-Donadey, F., et al. (2010). Intracerebral administration of CpG oligonucleotide for patients with recurrent glioblastoma: a phase II study. Neuro Oncol. *12*, 401–408. https://doi.org/10.1093/neuonc/nop047.

32. Karim, R., Palazzo, C., Evrard, B., and Piel, G. (2016). Nanocarriers for the treatment of glioblastoma multiforme: Current state-of-the-art. J. Contr. Release *227*, 23–37. https://doi.org/10.1016/j.jconrel.2016.02.026.

33. Meng, L., Wang, C., Lu, Y., Sheng, G., Yang, L., Wu, Z., Xu, H., Han, C., Lu, Y., and Han, F. (2021). Targeted regulation of blood-brain barrier for enhanced therapeutic efficiency of hypoxia-modifier nanoparticles and immune checkpoint blockade antibodies for glioblastoma. ACS Appl. Mater. Interfaces *13*, 11657–11671. https://doi.org/10.1021/acsami.1c00347.

34. Kadiyala, P., Li, D., Nuñez, F.M., Altshuler, D., Doherty, R., Kuai, R., Yu, M., Kamran, N., Edwards, M., Moon, J.J., et al. (2019). High-density lipoprotein-mimicking nanodiscs for chemo-immunotherapy against glioblastoma multiforme. ACS Nano *13*, 1365–1384. https://doi.org/10.1021/acsnano.8b06842.

35. Shankar, G.M., Kirtane, A.R., Miller, J.J., Mazdiyasni, H., Rogner, J., Tai, T., Williams, E.A., Higuchi, F., Juratli, T.A., Tateishi, K., et al. (2018). Genotype-targeted local therapy of glioma. Proc. Natl. Acad. Sci. USA *115*, E8388–E8394. https://doi.org/10.1073/pnas.1805751115.

36. Li, H., Somiya, M., and Kuroda, S. (2021). Enhancing antibody-dependent cellular phagocytosis by Re-education of tumor-associated macrophages with resiquimod-encapsulated liposomes. Biomaterials *268*, 120601. https://doi.org/10.1016/j.biomaterials.2020.120601.

37. Zhang, Y., Chen, Y., Li, J., Zhu, X., Liu, Y., Wang, X., Wang, H., Yao, Y., Gao, Y., and Chen, Z. (2021). Development of Toll-like receptor agonist-loaded nanoparticles as precision immunotherapy for reprogramming tumor-associated macrophages. ACS Appl. Mater. Interfaces *13*, 24442–24452. https://doi.org/10.1021/acsami.1c01453.

38. Liu, L., Wang, Y., Guo, X., Zhao, J., and Zhou, S. (2020). A biomimetic polymer magnetic nanocarrier polarizing tumor-associated macrophages for potentiating immunotherapy. Small *16*, e2003543. https://doi.org/10.1002/smll.202003543.

39. Ali-Boucetta, H., Bitounis, D., Raveendran-Nair, R., Servant, A., Van den Bossche, J., and Kostarelos, K. (2013). Purified graphene oxide dispersions lack in vitro cytotoxicity and in vivo pathogenicity. Adv. Healthcare Mater. *2*, 433–441. https://doi.org/10.1002/adhm.201200248.

40. Zhang, Q., Wu, Z., Li, N., Pu, Y., Wang, B., Zhang, T., and Tao, J. (2017). Advanced review of graphene-based nanomaterials in drug delivery systems: Synthesis, modification, toxicity and application. Mater. Sci. Eng., C *77*, 1363–1375. https://doi.org/10.1016/j.msec.2017.03.196.

41. Shin, Y., Vranic, S., Just-Baringo, X., Gali, S.M., Kisby, T., Chen, Y., Gkoutzidou, A., Prestat, E., Beljonne, D., Larrosa, I., et al. (2020). Stable, concentrated, biocompatible, and defect-free graphene dispersions with positive charge. Nanoscale *12*, 12383–12394. https://doi.org/10.1039/d0nr02689a.

42. Andrews, J.P.M., Joshi, S.S., Tzolos, E., Syed, M.B., Cuthbert, H., Crica, L.E., Lozano, N., Okwelogu, E., Raftis, J.B., Bruce, L., et al. (2024). First-in-human controlled inhalation of thin graphene oxide nanosheets to study acute cardiorespiratory responses. Nat. Nanotechnol. *19*, 705–714. https://doi.org/10.1038/s41565-023-01572-3.

43. Jasim, D.A., Newman, L., Rodrigues, A.F., Vacchi, I.A., Lucherelli, M.A., Lozano, N., Ménard-Moyon, C., Bianco, A., and Kostarelos, K. (2021). The impact of graphene oxide sheet lateral dimensions on their pharmacokinetic and tissue distribution profiles in mice. J. Contr. Release *338*, 330–340. https://doi.org/10.1016/j.jconrel.2021.08.028.

44. Portioli, C., Bussy, C., Mazza, M., Lozano, N., Jasim, D.A., Prato, M., Bianco, A., Bentivoglio, M., and Kostarelos, K. (2020). Intracerebral injection of graphene oxide nanosheets mitigates microglial activation without inducing acute neurotoxicity: A pilot comparison to other nanomaterials. Small *16*, e2004029. https://doi.org/10.1002/smll.202004029.

45. de Lázaro, I., Sharp, P., Gurcan, C., Ceylan, A., Stylianou, M., Kisby, T., Chen, Y., Vranic, S., Barr, K., and Taheri, H. (2021). Deep tissue translocation of graphene oxide sheets in human glioblastoma 3D spheroids and an orthotopic xenograft model. Advanced Therapeutics *4*, 2000109. https://doi.org/10.1002/adtp.202000109.

46. Sharp, P.S., Stylianou, M., Arellano, L.M., Neves, J.C., Gravagnuolo, A.M., Dodd, A., Barr, K., Lozano, N., Kisby, T., and Kostarelos, K. (2023). Graphene Oxide Nanoscale Platform Enhances the Anti-Cancer Properties of Bortezomib in Glioblastoma Models. Adv. Healthcare Mater. *12*, e2201968. https://doi.org/10.1002/adhm.202201968.

47. Yin, Y., Li, X., Ma, H., Zhang, J., Yu, D., Zhao, R., Yu, S., Nie, G., and Wang, H. (2021). *In Situ* Transforming RNA Nanovaccines from Polyethylenimine Functionalized Graphene Oxide Hydrogel for Durable Cancer Immunotherapy. Nano Lett. *21*, 2224–2231. https://doi.org/10.1021/acs.nanolett.0c05039.

48. Yin, Y., Nguyen, T.L., Wang, B., Duong, H.T.T., Lee, D.S., Kim, J.H., Kim, J., and Jeong, J.H. (2019). Simultaneous delivery of DNA vaccine and hydrophobic adjuvant using reducible polyethylenimine-functionalized graphene oxide for activation of dendritic cells. J. Ind. Eng. Chem. *80*, 870–876. https://doi.org/10.1016/j.jiec.2019.08.038.

49. Despotopoulou, D., Stylianou, M., Arellano, L.M., Kisby, T., Lozano, N., and Kostarelos, K. (2023). Engineering of a graphene oxide-based two-dimensional platform for immune activation and modulation. Preprint at bioRxiv. https://doi.org/10.1101/2023.08.22.553542.

50. Marklein, R.A., Lam, J., Guvendiren, M., Sung, K.E., and Bauer, S.R. (2018). Functionally-relevant morphological profiling: A tool to assess cellular heterogeneity. Trends Biotechnol. *36*, 105–118. https://doi.org/10.1016/j.tibtech.2017.10.007.

51. Bertani, F.R., Mozetic, P., Fioramonti, M., Iuliani, M., Ribelli, G., Pantano, F., Santini, D., Tonini, G., Trombetta, M., Businaro, L., et al. (2017). Classification of M1/M2-polarized human macrophages by label-free hyperspectral reflectance confocal microscopy and multivariate analysis. Sci. Rep. *7*, 8965. https://doi.org/10.1038/s41598-017-08121-8.

52. de Charette, M., Marabelle, A., and Houot, R. (2016). Turning tumour cells into antigen presenting cells: The next step to improve cancer immunotherapy? Eur. J. Cancer *68*, 134–147. https://doi.org/10.1016/j.ejca.2016.09.010.

53. Mantovani, A., Allavena, P., Sica, A., and Balkwill, F. (2008). Cancer-related inflammation. Nature *454*, 436–444. https://doi.org/10.1038/nature07205.

54. Prosniak, M., Harshyne, L.A., Andrews, D.W., Kenyon, L.C., Bedelbaeva, K., Apanasovich, T.V., Heber-Katz, E., Curtis, M.T., Cotzia, P., and Hooper, D.C. (2013). Glioma grade is associated with the accumulation and activity of cells bearing M2 monocyte markers. Clin. Cancer Res. *19*, 3776–3786. https://doi.org/10.1158/1078-0432.CCR-12-1940.

55. Steidl, C., Lee, T., Shah, S.P., Farinha, P., Han, G., Nayar, T., Delaney, A., Jones, S.J., Iqbal, J., Weisenburger, D.D., et al. (2010). Tumor-associated macrophages and survival in classic Hodgkin's lymphoma. N. Engl. J. Med. *362*, 875–885. https://doi.org/10.1056/NEJMoa0905680.

56. Pang, L., Khan, F., Dunterman, M., and Chen, P. (2022). Pharmacological targeting of the tumor–immune symbiosis in glioblastoma. Trends Pharmacol. Sci. *43*, 686–700. https://doi.org/10.1016/j.tips.2022.04.002.

57. Guerriero, J.L., Sotayo, A., Ponichtera, H.E., Castrillon, J.A., Pourzia, A.L., Schad, S., Johnson, S.F., Carrasco, R.D., Lazo, S., Bronson, R.T., et al. (2017). Class IIa HDAC inhibition reduces breast tumours and metastases through anti-tumour macrophages. Nature *543*, 428–432. https://doi.org/10.1038/nature21409.

58. Gu, Z., Zhu, S., Yan, L., Zhao, F., and Zhao, Y. (2019). Graphene-based smart platforms for combined Cancer therapy. Adv. Mater. *31*, 1800662. https://doi.org/10.1002/adma.201800662.

59. Fusco, L., Gazzi, A., Peng, G., Shin, Y., Vranic, S., Bedognetti, D., Vitale, F., Yilmazer, A., Feng, X., Fadeel, B., et al. (2020). Graphene and other 2D materials: a multidisciplinary analysis to uncover the hidden potential as cancer theranostics. Theranostics *10*, 5435–5488. https://doi.org/10.7150/thno.40068.

60. Mukherjee, S.P., Bottini, M., and Fadeel, B. (2017). Graphene and the immune system: a romance of many dimensions. Front. Immunol. *8*, 673. https://doi.org/10.3389/fimmu.2017.00673.

61. Sen, O.z., Emanet, M., Mazzuferi, M., Bartolucci, M., Catalano, F., Prato, M., Moscato, S., Marino, A., De Pasquale, D., and Pugliese, G. (2023). Microglia Polarization and Antiglioma Effects Fostered by Dual Cell Membrane-Coated Doxorubicin-Loaded Hexagonal Boron Nitride Nanoflakes. ACS Appl. Mater. Interfaces *15*, 58260–58273. https://doi.org/10.1021/acsami.3c17097.

62. Jasim, D.A., Murphy, S., Newman, L., Mironov, A., Prestat, E., McCaffrey, J., Ménard-Moyon, C., Rodrigues, A.F., Bianco, A., Haigh, S., et al. (2016). The effects of extensive glomerular filtration of thin graphene oxide sheets on kidney physiology. ACS Nano *10*, 10753–10767. https://doi.org/10.1021/acsnano.6b03358.

63. Newman, L., Rodrigues, A.F., Jasim, D.A., Vacchi, I.A., Ménard-Moyon, C., Bianco, A., Bussy, C., and Kostarelos, K. (2020). Nose-to-brain translocation and cerebral biodegradation of thin graphene oxide nanosheets. Cell Reports Physical Science *1*, 100176. https://doi.org/10.1016/j.xcrp.2020.100176.

64. Newman, L., Jasim, D.A., Prestat, E., Lozano, N., De Lazaro, I., Nam, Y., Assas, B.M., Pennock, J., Haigh, S.J., Bussy, C., and Kostarelos, K. (2020). Splenic capture and *In Vivo* intracellular biodegradation of biological-grade graphene oxide sheets. ACS Nano *14*, 10168–10186. https://doi.org/10.1021/acsnano.0c03438.

65. Vranic, S., Rodrigues, A.F., Buggio, M., Newman, L., White, M.R.H., Spiller, D.G., Bussy, C., and Kostarelos, K. (2018). Live imaging of label-free graphene oxide reveals critical factors causing oxidative-stress-mediated cellular responses. ACS Nano *12*, 1373–1389. https://doi.org/10.1021/acsnano.7b07734.

66. Rodrigues, A.F., Newman, L., Jasim, D., Mukherjee, S.P., Wang, J., Vacchi, I.A., Ménard-Moyon, C., Bianco, A., Fadeel, B., Kostarelos, K., and Bussy, C. (2020). Size-dependent pulmonary impact of thin graphene oxide sheets in mice: toward safe-by-design. Adv. Sci. *7*, 1903200. https://doi.org/10.1002/advs.201903200.

67. Narayanan, J.S.S., Ray, P., Hayashi, T., Whisenant, T.C., Vicente, D., Carson, D.A., Miller, A.M., Schoenberger, S.P., and White, R.R. (2019). Irreversible electroporation combined with checkpoint blockade and TLR7 stimulation induces antitumor immunity in a murine pancreatic cancer model. Cancer Immunol. Res. *7*, 1714–1726. https://doi.org/10.1158/2326-6066.CIR-19-0101.

68. Michaelis, K.A., Norgard, M.A., Zhu, X., Levasseur, P.R., Sivagnanam, S., Liudahl, S.M., Burfeind, K.G., Olson, B., Pelz, K.R., Angeles Ramos, D.M., et al. (2019). The TLR7/8 agonist R848 remodels tumor and host responses to promote survival in pancreatic cancer. Nat. Commun. *10*, 4682. https://doi.org/10.1038/s41467-019-12657-w.

69. Schmid, D., Park, C.G., Hartl, C.A., Subedi, N., Cartwright, A.N., Puerto, R.B., Zheng, Y., Maiarana, J., Freeman, G.J., Wucherpfennig, K.W., et al. (2017). T cell-targeting nanoparticles focus delivery of immunotherapy to improve antitumor immunity. Nat. Commun. *8*, 1747. https://doi.org/10.1038/s41467-017-01830-8.

70. Zahr, N.M., Zhao, Q., Goodcase, R., and Pfefferbaum, A. (2022). Systemic administration of the TLR7/8 agonist resiquimod (R848) to mice is associated with transient, in Vivo-detectable brain swelling. Biology *11*, 274. https://doi.org/10.3390/biology11020274.

71. Pockros, P.J., Guyader, D., Patton, H., Tong, M.J., Wright, T., McHutchison, J.G., and Meng, T.-C. (2007). Oral resiquimod in chronic HCV infection: safety and efficacy in 2 placebo-controlled, double-blind phase IIa studies. J. Hepatol. *47*, 174–182. https://doi.org/10.1016/j.jhep.2007.02.025.

72. Jasim, D.A., Ménard-Moyon, C., Bégin, D., Bianco, A., and Kostarelos, K. (2015). Tissue distribution and urinary excretion of intravenously administered chemically functionalized graphene oxide sheets. Chem. Sci. *6*, 3952–3964. https://doi.org/10.1039/c5sc00114e.

73. Bahmani, B., Gong, H., Luk, B.T., Haushalter, K.J., DeTeresa, E., Previti, M., Zhou, J., Gao, W., Bui, J.D., Zhang, L., et al. (2021). Intratumoral immunotherapy using platelet-cloaked nanoparticles enhances antitumor immunity in solid tumors. Nat. Commun. *12*, 1999. https://doi.org/10.1038/s41467-021-22311-z.

74. Lugani, S., Halabi, E.A., Oh, J., Kohler, R.H., Peterson, H.M., Breakefield, X.O., Chiocca, E.A.A., Miller, M.A., Garris, C.S., and Weissleder, R. (2023). Dual immunostimulatory pathway agonism through a synthetic nanocarrier triggers robust anti-tumor immunity in murine glioblastoma. Adv. Mater. *35*, 2208782. https://doi.org/10.1002/adma.202208782.

75. Cordell, E.C., Alghamri, M.S., Castro, M.G., and Gutmann, D.H. (2022). T lymphocytes as dynamic regulators of glioma pathobiology. Neuro Oncol. *24*, 1647–1657. https://doi.org/10.1093/neuonc/noac055.

76. Omuro, A., Vlahovic, G., Lim, M., Sahebjam, S., Baehring, J., Cloughesy, T., Voloschin, A., Ramkissoon, S.H., Ligon, K.L., Latek, R., et al. (2018). Nivolumab with or without ipilimumab in patients with recurrent glioblastoma: results from exploratory phase I cohorts of CheckMate 143. Neuro Oncol. *20*, 674–686. https://doi.org/10.1093/neuonc/nox208.

77. Reardon, D.A., Brandes, A.A., Omuro, A., Mulholland, P., Lim, M., Wick, A., Baehring, J., Ahluwalia, M.S., Roth, P., Bähr, O., et al. (2020). Effect of nivolumab vs bevacizumab in patients with recurrent glioblastoma: the CheckMate 143 phase 3 randomized clinical trial. JAMA oncology *6*, 1003–1010. https://doi.org/10.1001/jamaoncol.2020.1024.

78. Frederico, S.C., Hancock, J.C., Brettschneider, E.E.S., Ratnam, N.M., Gilbert, M.R., and Terabe, M. (2021). Making a cold tumor hot: The role of vaccines in the treatment of glioblastoma. Front. Oncol. *11*, 672508. https://doi.org/10.3389/fonc.2021.672508.

79. Abe, B.T., and Macian, F. (2013). Uncovering the mechanisms that regulate tumor-induced T-cell anergy. OncoImmunology *2*, e22679. https://doi.org/10.4161/onci.22679.

80. Philip, M., and Schietinger, A. (2022). $CD8^+$ T cell differentiation and dysfunction in cancer. Nat. Rev. Immunol. *22*, 209–223. https://doi.org/10.1038/s41577-021-00574-3.

81. Woroniecka, K.I., Rhodin, K.E., Chongsathidkiet, P., Keith, K.A., and Fecci, P.E. (2018). T-cell dysfunction in glioblastoma: applying a new framework. Clin. Cancer Res. *24*, 3792–3802. https://doi.org/10.1158/1078-0432.CCR-18-0047.

82. Mohme, M., Schliffke, S., Maire, C.L., Rünger, A., Glau, L., Mende, K.C., Matschke, J., Gehbauer, C., Akyüz, N., Zapf, S., et al. (2018). Immunophenotyping of newly diagnosed and recurrent glioblastoma defines distinct Immune exhaustion profiles in peripheral and tumor-infiltrating lymphocytes. Clin. Cancer Res. *24*, 4187–4200. https://doi.org/10.1158/1078-0432.CCR-17-2617.

83. Woroniecka, K., Chongsathidkiet, P., Rhodin, K., Kemeny, H., Dechant, C., Farber, S.H., Elsamadicy, A.A., Cui, X., Koyama, S., Jackson, C., et al. (2018). T-cell exhaustion signatures vary with tumor type and are severe in glioblastoma. Clin. Cancer Res. *24*, 4175–4186. https://doi.org/10.1158/1078-0432.CCR-17-1846.

84. Mullins, S.R., Vasilakos, J.P., Deschler, K., Grigsby, I., Gillis, P., John, J., Elder, M.J., Swales, J., Timosenko, E., Cooper, Z., et al. (2019). Intratumoral immunotherapy with TLR7/8 agonist MEDI9197 modulates the tumor microenvironment leading to enhanced activity when combined with other immunotherapies. J. Immunother. Cancer *7*, 244. https://doi.org/10.1186/s40425-019-0724-8.

85. Rodrigues, A.F., Newman, L., Lozano, N., Mukherjee, S.P., Fadeel, B., Bussy, C., and Kostarelos, K. (2018). A blueprint for the synthesis and characterisation of thin graphene oxide with controlled lateral dimensions for biomedicine. 2D Mater. *5*, 035020. https://doi.org/10.1088/2053-1583/aac05c.